

THESIS
2
1999



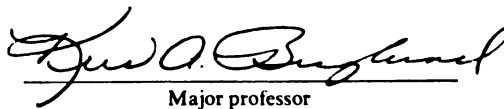
This is to certify that the
dissertation entitled
DEVELOPMENT OF SECOND HARMONIC GENERATION
AS A TOOL FOR MONITORING CRYSTALLIZATION

presented by

DALE JERRY LECAPTAIN

has been accepted towards fulfillment
of the requirements for

Ph.D. degree in CHEMISTRY


Major professor

Date Aug 13, 1999

**LIBRARY
Michigan State
University**

**PLACE IN RETURN BOX to remove this checkout from your record.
TO AVOID FINES return on or before date due.
MAY BE RECALLED with earlier due date if requested.**

DATE DUE	DATE DUE	DATE DUE
<hr/>	<hr/>	<hr/>

**Development of Second Harmonic Generation as a Tool for Monitoring
Crystallization**

By

DALE JERRY LECAPTAIN

A DISSERTATION

Submitted to

Michigan State University

in partial fulfillment of the requirements

for the degree of

DOCTOR OF PHILOSOPHY

Department of Chemistry

1999

ABSTRACT

DEVELOPMENT OF SECOND HARMONIC GENERATION AS A TOOL FOR MONITORING CRYSTALLIZATION

By

DALE JERRY LECAPTAIN

Crystallization is a widely used separation and purification process. However, the large number of variables affecting crystallization makes theoretical prediction of the process unreliable. Therefore, to obtain a large mean size, uniform crystal size distribution and efficient separation control of the crystallizer is necessary. This requires *in situ* monitoring of the system. The studies presented demonstrate Second Harmonic Generation (SHG) and Raman spectroscopy as useful techniques for monitoring batch crystallization.

Raman spectroscopy is demonstrated as a useful method for monitoring the change in solution structure, as well as the formation of crystals. Potassium dihydrogen phosphate has a red shift in the symmetric stretch of the phosphorous hydroxyl bond when transferring from solution to crystalline phase. Using this shift, a desupersaturation curve can be constructed.

The non-linear optical process of second harmonic generation (SHG) is a novel technique for this purpose. SHG is more sensitive, can be used *in situ*, and is less prone to interference than turbidometric, and light scattering methods. SHG is also orders of magnitude more sensitive than turbidity, resulting in 5-15 minutes shorter measured induction times than aforementioned techniques. The technique is demonstrated for measuring the induction time of an inorganic salt, a sugar, and an amino acid.

The probe configuration designed and discussed provides a practical way to monitor the crystallization process *in situ*, noninvasive, and in real time using SHG. Monitoring the crystallization using SHG provides a means for knowing when to control it, which is demonstrated on L-lysine monohydrochloride crystallization. A slight increase in the mean size and a drastic change in the crystal quality occur.

The SHG monitoring probe can differentiate between different polymorphs during crystallization. The SHG selectively detects polymorph crystal formation. *In situ* detection is possible of L-aspartic acid and L-glutamic acid. The former crystallizes in small particulate form and in a larger more regular form. The latter transforms from a small particulate form and transforms into the larger more regular form. By monitoring the crystal formation, relative efficiency of the two polymorphs, and preliminary work toward the incorporation of light scattering into the SHG analysis is possible.

Ease of sampling and response time of SHG makes it applicable to *in situ* determination of enantiomer crystallization. L-aspartic acid crystallization can be differentiated from DL aspartic acid crystallization using the SHG technique.

ACKNOWLEDGMENTS

First and foremost thanks are to my advisor Prof. Kris Berglund. His guidance and numerous ideas made this work possible and always kept it interesting. Never would a conversation end without a 'few' new ideas to think about. Also thanks to Prof. Gary Blanchard who would answer any question I would have. Thanks to the rest of my guidance committee too, Dean George Leroi and Prof. Alec Scranton.

Next up on the thanks list is Jen. Always there to hear the 'other' side of the story. Mom and Dad whose support was under appreciated, but still strongest when it counted most. My brothers and sisters, Mom and Dad 'in-law', the grandparents, thanks for listening, talking, supporting, praying, helping, etc.

Number three on the list is the friends that have shared this 'journey' and a beer or two. The list is long and the thanks run deep, but space only permits the ones dearest indeed. Wendy, thank you, Matt Leanne, ditto. Eric (Killer), Karen, Bob, Tom, Richard, Jeremy, Shannon, Daniels, LT and the list goes on.... Almost forgot Art, whose hours of counseling have meant a lot.

Last, but not least is those that most certainly need to be thanked and have had the 'privilege' of working with me. Dan Engebretson, for making the laser lab navigable. Dilum and Sanjay, for a discussion or three about crystallization. Prof. Kathy Hunt and Dr. Tom Carter for those bits of technical information. The rest of the labmates past and present; Mike, Adam, Carinna, Hasan, Fang, Al, Anna, Parminder, Lilli, Jennifer, Charles, Trisha, Marketta, Rob, Kitz, Borlan, Chris, Beatrice, and Laurie.

Finally, thank you for reading, I hope you read on to learn the rest of the story.

TABLE OF CONTENTS

List of Tables	viii
List of Figures	ix
List of Abbreviations	xv
Introduction	
DEVELOPMENT OF SECOND HARMONIC GENERATION AS A TOOL FOR MONITORING CRYSTALLIZATION	
.....	1
I.1 Crystallization	2
I.2 Second Harmonic Generation	12
I.3 <i>In Situ</i> Crystallization Studies	15
I.4 Overview	17
I.5 References	17
Chapter 1	
USING RAMAN SPECTROSCOPY FOR MONITORING POTASSIUM DIHYDROGEN PHOSPHATE BATCH CRYSTALLIZATION	
.....	21
1.1 Background	21
1.2 Experimental	22
1.3 Results and Discussion	24
1.4 References	29
Chapter 2	
THE APPLICABILITY OF SECOND HARMONIC GENERATION FOR <i>IN SITU</i> MEASUREMENT OF INDUCTION TIME OF SELECTED CRYSTALLIZATION SYSTEMS	
.....	30
2.1 Background	30
2.2 Experimental	32
2.3 Results and Discussion	36
2.4 Conclusions	43
2.5 References	47

Chapter 3

AN *IN SITU* SECOND HARMONIC GENERATION PROBE FOR MONITORING BATCH CRYSTALLIZATION OF LYSINE MONOHYDROCHLORIDE

.....	48
3.1 System Design	48
3.2 Application	52
3.3 Conclusions	61
3.4 References	61

Chapter 4

DETECTION OF POLYMORPH CRYSTALLIZATION AND TRANSFORMATION USING SHG

.....	62
4.1 Background	63
4.2 Experimental	64
4.2 Data and Discussion	66
4.4 Conclusions	84
4.5 References	93

Chapter 5

ENANTIOMERIC CRYSTAL DETERMINATION USING SHG

.....	94
5.1 Background	94
5.2 Experimental	95
5.3 Data and Discussion	96
5.4 Conclusions	101
5.5 References	101

Chapter 6

FUTURE WORK; SECOND ORDER NONLINEAR OPTICAL CHEMICAL SENSORS

.....	102
6.1 Introduction	102
6.2 Background	102
6.3 Experimental	103
6.5 References	106

Conclusion	107
APPENDIX	109

LIST OF TABLES

Table A.1	Data for Figure 1.4	110
Table A.2	Data for Figure 2.4	112
Table A.3	Data for Figure 3.5	112

LIST OF FIGURES

Figure I.1	Flow chart depicting the different types of nucleation and the corresponding subcategories.	3
Figure I.2	Temperature versus concentration showing various zones of a solubility curve. The solid line is the saturation limit and the dashed line is the metastable limit.	7
Figure I.3	Schematic showing a typical desupersaturation crystallization curve. The induction time indicates where crystal nucleation is detected in the latent time period. With crystal present nucleation and growth consume the available supersaturation causing the rapid drop in concentration. Finally, the solution returns to saturation.	9
Figure I.4	Flow chart illustrating the interaction of between size and kinetics for crystallization.	11
Figure 1.1	The experimental set-up including the Kaiser Optical HoloLab 1000 Raman Spectrophotometer and laboratory scale crystallizer.	23
Figure 1.2	The experimental set-up including the Kaiser Optical HoloLab 1000 Raman Spectrophotometer and laboratory scale crystallizer.	26
Figure 1.3	Stacked plot of Raman spectra for the KDP crystallization. The spectra are taken at 5 minute intervals starting at the front.	27
Figure 1.4	Peak intensity ratio of the KDP solution peak at 886 cm^{-1} and the crystalline peak at 917 cm^{-1}	28
Figure 2.1	Experimental set-up used for the SHG experiments.	33
Figure 2.2	Schematic of the experimental batch crystallizer, temperature controlled with solution pumping action. The operating solution volume is 390 mL.	35

Figure 2.3	<p>Typical Crystal Formation of potassium dihydrogen phosphate (8.9% supersaturated KDP at 30 °C). Region I: Supersaturated solution, no crystals Region II: Self-nucleation, crystals starting to form (induction time) Region III: Rapid desupersaturation, nucleation and crystal growth Region IV: Return to saturation, no more nucleation or growth 38</p>	38
Figure 2.4	<p>Isothermal induction times for varying concentrations of KDP supersaturated solutions. (% Supersaturated is the wt % over the saturation value.) All measurements were recorded at 29.7°C with the same 5-minute cool down to supersaturation level. 39</p>	39
Figure 2.5	<p>SHG monitoring of 35.4% supersaturation α-Lactose crystal formation. The crystallization was performed isothermally at 20 °C. The maximum and subsequent decrease in measured intensity is due to scatter from the large quantity of crystals. 41</p>	41
Figure 2.6	<p>SHG(O) and light scatter(X) monitoring of L-lysine-HCl. The SHG is normalized to the amount of SHG detected, whereas the light scatter is the amount scattered with the saturated solution being the zero measure. The data shown is 200g lysine m-HCl dissolved into 300g water, and then cooled to 20 °C. The addition of 30 mL of ethanol occurs at the 5-minute mark. 42</p>	42
Figure 2.7	<p>Comparison of the induction time measurement using SHG (O) and light scatter (X) on crystallization curve of 7.53% supersaturated solution of KDP. 45</p>	45
Figure 2.8	<p>Expansion of figure 2.7 focusing on the early time measurement. The intensity is increased for the two methods to near the data scatter limit. 46</p>	46
Figure 3.1	<p>General schematic showing the experimental design. A pulsed laser provides the incident 1064 nm lights measured using a PMT. The sampling probe is detailed in figure 3.2. 49</p>	49

Figure 3.2	Laboratory scale (~400mL) crystallizer that has the SHG probe immersed to show the details of the design. The system design section describes the components in detail.	51
Figure 3.3	Cooling curve for L-lysine monohydrochloride controlled crystallization shown in figure 3.4. The control occurs at 21 minutes when the cooling is stopped in response to crystal detection.	54
Figure 3.4	SHG output from a typical L-lysine monohydrochloride crystallization. Temperature induced crystallization of a 80 g. in 150 mL water / 100 mL ethanol solution. The cooling profile is shown in figure 3.4.	56
Figure 3.5	Crystal population size distribution for L-lysine monohydrochloride showing slightly larger mean size for the controlled (square) experiments versus the reference (x) crystallization.	58
Figure 3.6	Photo of the L-lysine monohydrochloride crystals sampled from the 390 micron average crystal size tray (mesh #45) of the controlled crystallization.	59
Figure 3.7	Photo of L-lysine monohydrochloride sampled from the reference experiment (390 micron average crystal tray). Agglomerates dominate the sample with a small quantity of uniform crystals produced.	60
Figure 4.1	Schematic showing the light scattering set-up and equipment.	67
Figure 4.2	SHG signal showing the Anti-solvent (methanol) crystallization of a 1.8% wt. in water at 50°C of L-aspartic acid (Form A).	68
Figure 4.3	Photo of a sample of L-aspartic acid crystals collected after completion of the crystallization (Form A).	70

Figure 4.4	SHG output measured for the 1.4% wt. in water L-aspartic acid (Form B) anti-solvent crystallization at 10 °C. Changing optical properties of the solution causes the small fluctuation at the start. Through the course of the rapid crystallization no SHG is produced.	71
Figure 4.5	Light scattering curve for L-aspartic acid crystallization (Form B) measured simultaneously with figure 4.5. At 3 minutes methanol addition was started and at 28 minutes the crystal formation starts.	72
Figure 4.6	Photo shows the L-aspartic acid crystals (Form B) taken at the completion of the second experiment. The crystals appear as a very fine powder.	73
Figure 4.7	X-ray powder pattern shows the difference in the two L-aspartic acid crystals. The gray pattern (upper) corresponds to the non-SHG active crystal form (Form B, figure 4.6) and the black trace (lower) corresponds to the SHG active crystal (Form A, figure 4.2).	74
Figure 4.8	SHG crystal formation curve for the anti-solvent crystallization of 2.4% wt. in water L-glutamic acid at 20°C. Procedure A from the experimental section was used. Samples were collected and photographed at 17.4 minutes and at the completion of the experiment.	76
Figure 4.9	Photo of α crystals and small particles sampled at 17.4 minutes just after the start of the L-glutamic acid crystallization.	77
Figure 4.10	Photo of L-glutamic acid crystals, taken at the completion of the crystallization in figure 4.8. Shows the α form of crystals.	78
Figure 4.11	Plot shows the SHG anti-solvent crystallization of 2.8% wt. in water α L-glutamic acid. Crystal formation starts at 32 minutes. Solution samples were taken at 21 and 41 minutes.	79
Figure 4.12	Photo of L-glutamic acid small crystals taken at 21 minutes. The crystallization curve is shown in figure 4.7. The crystals are α form as determined by x-ray (figure 4.22).	80

Figure 4.13	Photo from the L-glutamic acid crystallization sampled at 41 minutes. Shows predominantly β crystals.	81
Figure 4.14	Photo from the L-glutamic acid crystallization, sample was collected upon completion of the experiment. Again, β crystals dominate.	82
Figure 4.15	SHG crystal formation of 3.3% wt. in water L-glutamic acid at 45°C generated using procedure C. The monitoring was extended to allow for transformation from the α form to the β form.	85
Figure 4.16	Photo of predominantly α L-glutamic acid crystals collected at time 69.1 minutes from the crystallization in figure 4.15.	86
Figure 4.17	L-glutamic acid crystals collected at the end of the experiment pictured in figure 4.15. Photo shows a near equal mix of α and β crystal forms.	87
Figure 4.18	SHG (o) crystal formation and light scattering (x) plotted for L-glutamic acid formation. The crystallization parameters are described as procedure C in the experimental section. Methanol addition was started at 3.1 minutes and samples were collected at 28.5 and 50.5 minutes.	88
Figure 4.19	L-glutamic acid crystals sampled at 28.5 minutes. The crystals are a mix of small particulate, α polymorph (prism), with a trace of the β form (needles).	89
Figure 4.20	L-glutamic acid crystal photographed at 28.5 minutes. The crystal shape is predominantly the α polymorph.	90
Figure 4.21	L-glutamic acid crystals collected at the completion of the experiment. Crystal shape is the prismatic α polymorph.	91
Figure 4.22	X-ray powder patterns for L-glutamic acid. Pattern 1 is crystals collected from crystallization of α form crystallization 4.11, pictured in figure 4.13. Pattern 2 is prism shape (α form) and pattern 3 is the needle shape as	

referenced.¹² Pattern 4 is crystals collected from 4.11 crystallization and pictured in figure 4.12.

	92
Figure 5.1	The SHG crystal formation curve for L-aspartic acid. Crystal formation starts at ~15 minutes and reaches depletion of the supersaturation at 23 minutes. Methanol as the anti solvent was used on this 1.9% wt/wt solution crystallized at 30 °C.	97
Figure 5.2	Photograph of L-aspartic acid crystals collected after the completion of the crystallization performed in figure 5.1. The crystals are rather small and difficult to fully contrast in this photo reproduction.	98
Figure 5.3	Photograph of L-aspartic acid crystals collected after the completion of the crystallization performed in figure 5.1. The crystals are rather small and difficult to fully contrast in this photo reproduction.	99
Figure 5.4	DL-aspartic acid crystals photographed upon completion of the crystallization. Distinct crystal shapes are present.	100
Figure 6.1	The schematic of an SHG sensor.	104

LIST OF ABBREVIATIONS

a_i	activity of species i
B^0	nucleation rate
ΔC	supersaturation
cm^{-1}	wavenumber
χ_n	n^{th} order susceptibility
E	energy
Eff	second harmonic efficiency
G	crystal growth rate
γ_i	ionic strength coefficient of species i
Hz	hertz
k_g	crystal growth rate constant
k_N	nucleation rate constant
i	to the i^{th} power
$I_{2\omega}$	second harmonic intensity
j	to the j^{th} power
k	propagation constant
k	to the k^{th} power
k_α	x-ray wavelength
KDP	potassium dihydrogen phosphate
L	crystal size
Lmhc	L-lysine monohydrochloride
m_i	molality of species i
mL	milliliter
M_T	suspension density
$\Delta\mu$	change in chemical potential
$\mu_i^0(T)$	standard chemical potential
$\mu_i(T)$	chemical potential
n	population density
nm	nanometer
η_ω	refractive index at ω
$\eta_{2\omega}$	refractive index at 2ω
P	polarization
PIR	peak intensity ratio
R	gas constant
ρ	density
s	supersaturation
S	size
SHG	second harmonic generation
σ	supersaturation
t	time
T	temperature
V	volume of crystals and solution

W	agitation rate
ω	frequency
z	direction

INTRODUCTION

DEVELOPMENT OF SECOND HARMONIC GENERATION AS A TOOL FOR MONITORING CRYSTALLIZATION

Batch crystallization is a widely used and efficient separation process for the production and purification of pharmaceuticals, food, and fine chemicals. Uniform crystals are desired for product consistency and for easier handling relative to fine powders. Efficient control of the crystallization process is necessary for obtaining large crystal mean size, narrow size distribution, and uniform purity. These characteristics provide good flow for handling and packaging, uniform final product appearance, and an economically feasible process. If allowed to progress in an uncontrolled manner crystallization can result in a predominantly fine powder with a wide size distribution. The crystallizer geometry, operating temperature, stirring rate, etc. all influence the crystallization process. No single theory of nucleation, growth, or molecular configuration of supersaturated solutions has a sufficient predictive value for process design. The independent variables of the process and difficulties in modeling play a role in the efficiency of control.

The real time monitoring of a crystallization process is critical for efficient control. To minimize contaminating the system and ensure efficiency, monitoring needs to be *in situ* and within the time frame of the phenomena. Many difficulties are associated with removing small samples of supersaturated solution and trying to make

sensitive measurements without changes occurring making the sample unrepresentative of the crystallizer. Perturbation to the crystallizing system must be kept to a minimum so as not to cause unnecessary disturbances that could affect the process and ultimately the final product. Lastly, the measurements of the crystallization properties need to be made within the time frame of the phenomenon so that control can be exercised. A long data collection time would give results too late for useful control.

The importance and challenges of crystallization are introduced above. At this point a common basis in accepted crystallization principles and terms as used throughout the remainder of the text is presented.

I.1 CRYSTALLIZATION

Crystallization proceeds by first the formation of nuclei and followed by growth. The crystallization process is a combined kinetic, thermal, and mass transfer phenomenon. The two primary steps of crystallization, nucleation and growth, require a supersaturated solution. A supersaturated solution contains more than the equilibrium amount of solute at a given temperature.

The first step in the crystallization process is the nucleation of crystals from the solution. Illustrated in the flow chart are the two types of nucleation. Primary nucleation is the formation of crystals from solution. Chemical potential overload of the solution causes homogenous nucleation, whereas foreign particles, which can be in the solution or part of the crystallizer cause heterogeneous nucleation. Secondary nucleation occurs when new crystals form from growing crystals in the solution.¹ The formation mechanisms have been studied with no definitive model developed. Though no

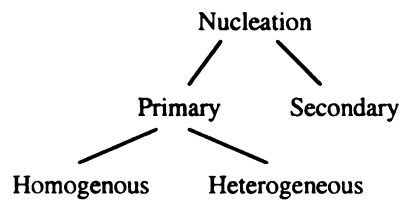


Figure I.1

Flow chart depicting the different types of nucleation and the corresponding subcategories.

mechanism is accepted several correlations of nucleation kinetics have satisfactorily described by experimental data.

$$B^o = k_N W^i M_T^j (\Delta C)^k$$

Where the nucleation rate (B^o) is proportional to the agitation rate (W) in rpm, suspension density (M_T) in mass per volume, and the supersaturation (ΔC). The dependence on agitation, suspension density, and supersaturation is realized because most nuclei in an industrial crystallizer are generated by contact with the crystallizer environment.¹

The molecular composition of the solution creates a gray area between nucleation and growth mechanisms. The small size, randomness, and motion of the solution/slurry in a crystallizer make direct measurement difficult. The two common theories regarding nucleation are; 1 the crystals nucleate as miniature crystals and that there is a diffuse body of molecules similar to the bulk surrounding that nucleus, 2 no clearly defined surface or boundary exists from where the nuclei eventually forms.^{2,3}

The first theory would be an assembly of one, then two, three molecules etc. until the critical nucleus size forms.⁴ The primary support for these studies was done using concentration gradients⁵, diffusion⁶, and Raman⁷. The size of these critical nuclei has been proposed by Larson and Garside to be clusters 2 to 10 nanometers. Alternatively, agitation, convection, or even Brownian motion provides the energy necessary to form critically sized nuclei.⁶

The second crystal nucleation theory could be considered a hydrate where the solvent molecules are pushed out for crystal formation. Supporting this Chakraborty and Berglund show that aqueous sucrose molecules form an envelope of solute, which encases the water molecules. Therefore, the requirement for nucleation is the expulsion

of the water.⁸ An alternative way of determining this is by measuring the rotational reorientation time using fluorescence lifetimes. Cluster size can be approximated and in turn determine the quantity of solvent trapped. This requires a fluorescent molecule that binds to the crystallizing species.⁹

The second step in the crystallization process is crystal growth. The requirements for growth are the presence of supersaturation and stable nuclei. At the microscopic level growth rate is irregular, but at the macro level growth rates are regular.¹⁶ The growth process has been thoroughly for several crystal systems.¹⁰ Several models such as 2-D growth, Burton-Cabrera-Frank Model, and the diffusion layer have been developed. These models provide a theoretical basis for correlation of experimental data for determination of kinetic parameters. The expression relating growth to supersaturation is

$$G = k_g \Delta C^i$$

This relates the growth rate (G) to the supersaturation (C) level. The equation uses the linear growth velocity as the basis.¹

The induction time is the period of time that elapses between achievement of supersaturation and the appearance of crystals.¹ Two processes, the formation of nuclei and the growth of crystals to a detectable size, make up this time period. The induction time is not an experimental characteristic of the system, but rather a way of monitoring a particular crystallization. A study by Söhnel and Mullin has shown that relative nucleation and growth rates can be established, but caution should be exercised when verifying the validity of such measurements.^{11,17} Determination of induction time is entirely dependent on how the crystals are detected. More efficient crystal detection

would measure a shorter induction time. The discrepancy in nucleation theories and inability of detection make the prediction of induction times nearly impossible.

Chemical potential difference is the driving force of crystallization. Extensive calculations have been done to relate chemical potential to the free energy of the system and are based on the classical works of Gibbs^{12,15} The chemical potential is related to concentration through the following for a given species i.

$$\mu_i(T) = \mu_i^{\circ}(T) + R T \ln (a_i)$$

The chemical potential (μ_i) relates to the standard chemical potential (μ_i°) and activity (a_i). The activity is related through the ionic strength coefficient (γ_i) to the molality (m_i).

$$a_i = m_i * \gamma_i$$

The molality though not trivial can be converted to the desired concentration units.¹³

Calculation of ionic strength is impractical because of the large concentrations associated with crystallization. Therefore supersaturation is used for reference in a crystallizing system.

A way to implement the concept of supersaturation is consider a solubility curve shown in figure I.1. The saturation line divides the stable region from the metastable region. Crystal formation cannot occur in the stable region and any crystals present will dissolve. The upper left region is the labile, where solute must come out of the solution. Supersaturated solutions exist in the metastable region, where crystal growth occurs. The further left and above the saturation line, the higher the supersaturation. Factors that affect zone width are the stirrer speed, cooling rate, evaporation rate, amount of impurities, the size and number of seed crystals, etc. An important point to keep in mind

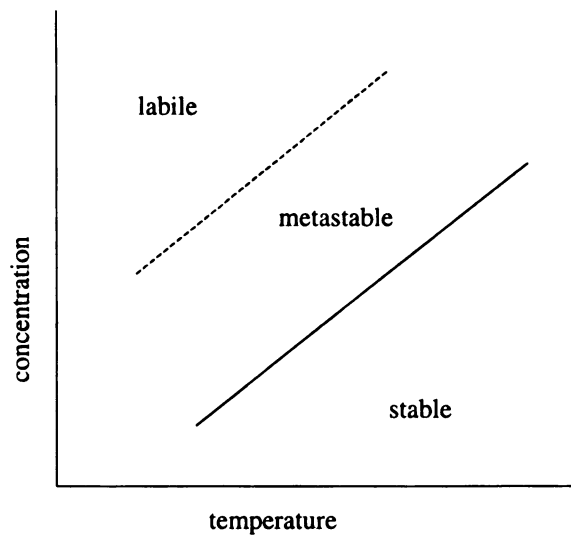


Figure I.2

Temperature versus concentration showing various zones of a solubility curve. The solid line is the saturation limit and the dashed line is the metastable limit.¹⁴

about the zone width is that it too is a function of the way in which the crystals are detected.^{2,3}

Traversing within the metastable region described above dictates the progress of the crystallization. Figure I.2 shows the crystallization curve for a batch cooling crystallization. The latent period consists of a supersaturated solution with no detectable nuclei present. Nucleation is the first step. The two common methods for providing crystal surface are in an industrial batch crystallizer are to either seed the supersaturated solution or increase the supersaturation to cause self-nucleation. Seeding is favorable because of a lower required supersaturation. The drawbacks of seeding are that an additional process step and guaranteeing the crystal seed quality are necessary.¹⁵ Once nucleation or seeding has occurred growth can occur. These two processes provide the means of desupersaturation. Crystal formation returns the solution to saturation, which will be at equilibrium with the crystals present.

The next consideration for the crystallization is final product. Specifically, quantifying and understanding the relationship between nucleation, growth, and supersaturation can be done considering the population balance. For a batch crystallizer the population balance can be reduced to the following.

$$\delta n / \delta t + V [\delta(G n) / \delta L] = 0$$

Where V is the volume of crystals and solution and is assumed to be well mixed so population density and supersaturation are constant. G is the growth rate, n the population density, t is time, and L the crystal size.¹⁶

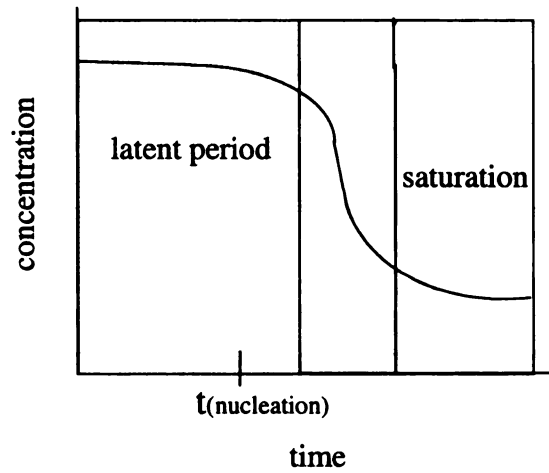


Figure I.3

Schematic showing a typical desupersaturation crystallization curve. The induction time indicates where crystal nucleation is detected in the latent time period. With crystal present nucleation and growth consume the available supersaturation causing the rapid drop in concentration. Finally, the solution returns to saturation.

Tying the experimental growth kinetics and nucleation kinetics provide a means for observing the crystallization. The growth and nucleation ultimately are a function of the supersaturation or driving force.

$$G \propto s^i \quad B^o \propto s^k$$

The kinetic orders for these processes i and k are system specific and typically are close to one for i and between three and five for k . Consequentially, at high supersaturation (s) the nucleation is favored.¹⁷

Ultimately batch crystallization can be broken down as follows. The supersaturation is the point of external system control and the starting point for this discussion. The common methods for changing supersaturation levels are through changing temperature, removing solvent, changing solvent composition, or the reaction rate. A small supersaturation (low $\Delta\mu$) favors growth and a large supersaturation (large $\Delta\mu$) favors nucleation. The nucleation rate is kinetically higher order than growth, which at high supersaturation drives nucleation more. Additionally, a large supersaturation (large $\Delta\mu$) increases the effect of system parameters such as crystallizer shape, agitation, temperature variations, etc., has on the nucleation. The quantity of nucleation versus growth determines the population density. The population density is the number of crystals per unit volume of the given size L . A large population density will have a large surface area. This large surface area permits rapid depletion of the supersaturation. Ideally a small surface area is desired so the small number of crystals can grow. But if the supersaturation is high, nucleation again starts to dominate.¹⁷

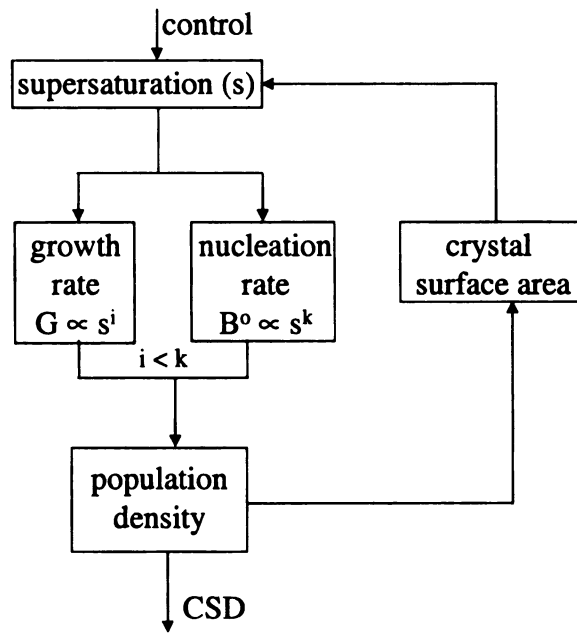


Figure I.4

Flow chart illustrating the interaction of between size and kinetics for crystallization.¹⁷

The premise for obtaining large mean crystal size requires keeping the supersaturation low to limit the nucleation and promote crystal growth. As an example a self-nucleation system needs to start with a high supersaturation for nucleation to occur. As soon as nuclei are present the supersaturation must be lowered so the growth can dominate. The strategy will produce larger crystals than an uncontrolled case.

I.2 SECOND HARMONIC GENERATION

Second Harmonic Generation (SHG) is the nonlinear conversion of two photons (frequency ω) to a single photon (frequency 2ω). It is the interaction of the electromagnetic wave dipole and the dipole of the medium. The medium has to have a dipole within the coherence length of the electromagnetic radiation for this phenomenon to occur. SHG is an optical method, therefore it can be used *in situ* and it is noninvasive to the system being measured. A review article by Corn and Higgins illustrates the extensive development SHG has had in the past fifteen years as an analytical tool for probing surfaces and interfaces.¹⁸ In particular, the experimental requirements for liquid interface studies^{19,20} are closely related to a batch crystallization setting. The key to the process is the absence of inversion symmetry within the coherence length of the laser pulse.

A practical understanding of light propagation through a dielectric medium is necessary for determining applicability of SHG. As an electromagnetic wave, described by Maxwell's equations, propagates through a dielectric medium a linear polarization is induced in the medium:²¹

$$P = \chi^{(1)} E$$

Where P is the polarization of the medium, $\chi^{(1)}$ is the susceptibility, and E is the energy of the electromagnetic wave. When the intensity of the incident electromagnetic wave is large enough a nonlinear response occurs in the medium. The resultant power series expansion of the polarization is shown below.

$$P = \chi^{(1)} E + \chi^{(2)} E^*E + \chi^{(3)} EE^*E + \dots$$

Inherently, the magnitude of χ_1 is much greater than $\chi^{(2)}$, which is much greater than $\chi^{(3)}$. Therefore, in large electromagnetic field intensities the $\chi^{(2)}$ response can be detected.

Substitution of the equation for an electric field ($E = E_0 \cos(\omega t - kz)$) illustrates the harmonic frequencies at 2ω , 3ω as well as ω of the incident wave. Where ω is the frequency, t is time, k the propagation constant, and z the direction.

$$P = \chi^{(1)} E_0 \cos(\omega t - kz) + 1/2 \chi^{(2)} E_0^2 [1 + \cos(2\omega t - 2kz)] + \text{higher order}$$

The second order term has two components, a DC response and a frequency doubling response. The doubled frequency (2ω) is the component of interest for optical second harmonic generation.²²

The conservation of energy requires that the second order ($\chi^{(2)}$) response occur only in anisotropic media. A symmetric medium has the same $\chi^{(2)}$ response for a positive and a negative electric field, therefore no net polarization occurs. Conversely, a non-symmetric medium has a different $\chi^{(2)}$ response for a positive and negative E-field, producing a $\chi^{(2)}$ response. A $\chi^{(2)}$ response is evidenced by the generation of the doubled light frequency.²²

The intensity of the second harmonic is dependent on several factors. The inherent properties of the crystal are constant. The second harmonic intensity is $I_{2\omega}$, ρ is

the density of the crystal, and S is the size of the crystal. The Efficiency of the crystal is a function of the phase matching and the wavelength being used.

$$I_{2\omega} \propto \rho S \text{ Eff}$$

A phase matching crystal system has the propagation constant at the second harmonic equal to the propagation constant at the incident wavelength. This can be related to the refractive indexes. Therefore when refractive index of the medium at ω (n_{ω}) equals the refractive index of the medium at 2ω ($n_{2\omega}$) the system is phase matched. Each face of a crystal has a different refractive index, which makes the intensity dependent on the face of the crystal being illuminated. The case where n_{ω} does not equal $n_{2\omega}$ is the non-phase matching condition. These may still be SHG active, but now depend heavily on the coherence length of the electromagnetic field.²³ The two alternative non-phase matching methods that exist in literature are Cerenkov radiation and quasi-phase-matching type I and II respectively. Type I uses lithium niobate waveguides where the end-faces are coated for high reflectivity of both incident and second harmonic and the temperature is tuned to form a resonator at both frequencies.²⁴ Type II involves a media where the refractive index is large enough so the second harmonic is radiated into the bounding medium.^{25,26}

The number and the size of particles also contribute to the SHG intensity. The polarization and incident energy are related quadratically, therefore the increase in size will go with the square of the intensity. The intensity of the second harmonic increases linearly with the number of crystals.³¹

A nanosecond or picosecond Nd/YAG laser produce an intense enough electric field for the second harmonic process to occur. The 1064 nm line is easiest to obtain and

therefore most often chosen, but is not required. Additionally, because of the frequency difference between the fundamental and second harmonic, filtering is quite efficient. Also the response of a conventional PMT is more efficient at 532 nm than at 1064 nm. The data collection necessary is the change in intensity of the doubled frequency.

There has been extensive work done on non-linear optical materials for the purpose of laser optical material development. As the availability and use of laser expanded so did the drive for understanding non-linear optical materials.^{27,28,29,30} The original work by Kurtz and Perry demonstrated SHG from crystal powder systems.³¹ This was expanded upon in the development of a screening method of potential crystal systems for laser optics.^{32,33} A review of the nonlinear efficiencies of organic crystals by Oudar and Zyss emphasizes this point.^{34,35} This powder technique was extended for use as a screening tool for determining the presence or absence of symmetry as a prelude to x-ray crystallography calculations.^{33,36}

I.3 *IN SITU* CRYSTALLIZATION DETECTION

In situ as defined by the Webster Dictionary is “in the natural or original position”.³⁷ This common definition does not provide adequate detail for specific ideas relevant to industrial batch crystallization, therefore it is expanded for this work. When using the term throughout the text the following definition needs to be kept in mind. The basic requirements that needs to be met are contact with the system should be kept to a minimum, no sample removal or excessive handling, and the response needs to be instantaneous relative to the experiment time scale. Additionally, from a practical standpoint the technique should be robust and sensitive to handle industrial conditions.

Monitoring crystallization can be accomplished through a variety of methods. Measuring the exothermic response due to the heat of crystallization is impractical due to the scale factor and measuring refractive index is impractical on slurries. Optical methods are non-intrusive and can offer a higher degree of reproducibility. A sampling of these studies include FTIR-ATR³⁸, fluorescence³⁹, and Raman spectroscopy.⁴⁰ These techniques may require various chemometric methods as they measure the supersaturation level. This direct link to the driving force provides intricate information about the crystallization. The variety of methods available lends themselves to potentially different systems, as development of a variety of techniques is necessary since no single technique works for all systems.

Instead of measuring the supersaturation level the appearance of crystals can be measured. The intuitive methods for measuring the crystals are visual and light scattering.⁴¹ Visual monitoring is analytically inefficient and light scattering suffers from interference from bubbles or other foreign particles in the system. These problems cause lower sensitivity and incorrect measurements.

Conventional methods for monitoring the onset of nucleation are based on light scattering, diffraction, or reflection. These techniques are prone to interference from dirt, air bubbles, changing solution consistency or a combination therein, which are very prevalent in industrial crystallizers. The physical differences of compounds and different types of crystallizers⁴² also make a universal technique for monitoring the process difficult.

I.4 OVERVIEW

Monitoring the formation of crystals can provide a way to refine models and aid in the control of crystallization. The novel proposed application of SHG provides a potentially better way for monitoring crystallization.

Laser optic research forms the basis for SHG monitoring of crystals. The focus there was to find materials for development of laser materials using large single crystal systems or well graded and prepared powders in refractive index controlled laboratory settings. The initial groundwork here was the design and set-up of systems that could be used in an industrial crystallization. Viscous and slurry solutions needed to be controlled for exposure with the laser light necessary for the second harmonic process.

The work is laid out roughly in the order of development. The exception is chapter 1, which deals with monitoring crystallization, but employs the use of Raman spectroscopy instead of SHG. Chapter 2 is the initial demonstration and proof of the technique applicability. In Chapter 3, refinements are presented and demonstrations of the technique in control are shown. Chapters 4 and 5 demonstrate the versatility of SHG for monitoring crystallization as polymorphic systems are studied as well as enantiomeric crystal systems. The final chapter is proposed research using SHG as an analytical sensor employing some of the groundwork laid out here.

I.5 REFERENCES

¹ Myerson, A. S. and Ginde, R., Handbook of Industrial Crystallization, Edt. Myerson, A. S, Butterworth-Heinemann, Boston, 1993

² Jense, A. H. and De Jong, E. J., *Trans. IChemE.*, 1978, 56, 187

- ³ Mullin, J. W. and Jancic, S. J., *Trans. IChemE.*, **1979**, 57, 188
- ⁴ Larson, M. A., Advances in Industrial Crystallization, Garside, J., Davey, R. J., and Jones, A. G.: ed., Butterworth-Heinemann Ltd., Oxford, **1991**,
- ⁵ Mullin, J. W. and Leci, C. L., *Correspondence*, **1969**, 1075; Larson, M. A. and Garside, J., *J. of Cryst. Growth*, **1986**, 76, 88
- ⁶ Larson, M. A. and Garside, J., *Chem. Eng. Science*, **1986**, 41, 1285
- ⁷ Frost, R. L. and James, D. W., *J. Chem. Soc., Faraday Trans. 1*, **1982**, 72, 3235; Rusli, I. T., Shcrader, G. L., and Larson, M. A., *J. of Cryst. Growth*, **1989**, 97, 345; Cerreta, M. K. and Berglund, K. A., *J. Cryst. Growth*, **1987**, 84, 577
- ⁸ Chakraborty, R. and Berglund, K. A., *J. of Cryst. Growth*, **1992**, 125, 81
- ⁹ Rasimas, J. P., Berglund, K. A., and Blanchard, G. J., *J. Phys. Chem.*, **1996**, 100: (42) 17034
- ¹⁰ Baird, J. K., Hill, S. C., Clunie, J.C., *J. of Cryst. Growth*, **1999**, 196, 220; Him, S. J. and Myerson A.S., *Indust. Eng. Chem. Res.*, **1996**, 35, 1078; Mydlarz, J. and Jones, A. G., *Chem. Eng. J. Bioch. Eng.*, **1994**, 55, 69; Garside, J., Gilbilaro, L. G., and Tavare, N. S., *Chem. Eng. Sci.*, **1982**, 37, 1625; Joshi, M. S., Antony, A.V., *J. of Phys. D Appl. Phys.*, **1977**, 17, 2393
- ¹¹ Söhnel, O. and Mullin, J. W., *J. of Colloid and Interface Science*, **1988**, 123, 43
- ¹² Gibbs, J. W., Collected Works Volume 1, Thermodynamics, Yale University Press, New Haven, **1948**
- ¹³ Myerson, A. S., Handbook of Industrial Crystallization, Edt. Myerson, A. S., Butterworth-Heinemann, Boston, **1993**
- ¹⁴ Mersmann, A., Crystallization Technology Handbook, Marcel Dekker Inc., New York, **1995**, Chaps. 1&2
- ¹⁵ Mullin, J. W., Crystallization, Butterworth-Heinemann, Oxford, **1993**, Chaps. 1-5
- ¹⁶ Wankat, P. C., Rate Controlled Separations, Elsevier Science Publisher, London, **1990**, Chaps. 3&4
- ¹⁷ Berglund, K. A., Handbook of Industrial Crystallization, Edt. Myerson, A. S., Butterworth-Heinemann, Boston, **1993**

- ¹⁸ Corn, R. M. and Higgins D. A., *Chem. Rev.*, **1994**, 94, 107
- ¹⁹ Conboy, J. C., Dashcbach, J. L., and Richmond, G. L., *J. Phys. Chem.*, **1994**, 98, 9688
- ²⁰ Kott, K. L., Higgins, D. A., McMahon, R. J., and Corn, R. M., *J. Am. Chem. Soc.*, **1993**, 115, 5342
- ²¹ Shen, Y. R., *The Principles of Nonlinear Optics*, John Wiley & Sons, Inc., New York, **1984**, pp. 1-11
- ²² Prasad, P. N. and Williams, D. J., *Introduction to Nonlinear Optical Effects in Molecules & Polymers*, John Wiley & Sons Inc., New York, **1991**
- ²³ Agrawal, G. P. and Boyd, R. W., *Contemporary Nonlinear Optics*, Academic Press Inc., San Diego, **1992**, Chaps 1 & 2
- ²⁴ Taniuchi, T., and Yamamoto, K., *CLEO Digest*, Paper WR3, **1986**
- ²⁵ Lim, E. J., Fefer, M. M., and Byer, R. L., *Electron. Lett.*, **1989**, 25, 174
- ²⁶ Webjorn, J., Laurell, F., and Arvidsson, G., *IEEE J. Lightwave Tech.*, **1989**, 7, 1597
- ²⁷ Edited by Chemla, D.S. and Zyss, J., *Nonlinear Optical Properties of Organic Molecules and Crystals Volume I*, Orlando, Academic Press, **1987**
- ²⁸ Wagnière, G. H., *Linear and Nonlinear Optical Properties of Molecules*, Weinheim, New York, **1993**
- ²⁹ Marder, S. R., Editor Sohn, J. E., and Stucky, G. D., *Materials for Nonlinear Optics Chemical Perspectives*, Washington DC, **1991**
- ³⁰ Prasad, P. N. and Williams, D. J., *Introduction to Nonlinear Optical Effects in Molecules and Polymers*, New York, Wiley, **1991**
- ³¹ Kurtz, S. K. and Perry, T. T., *J. of Appl. Phys.*, **1968**, 39, 3798
- ³² Dougherty, J. P. and Kurtz, S. K., *J. Appl. Cryst.*, **1976**, 9, 145
- ³³ Coda, A. and Pandarese, F., *J. Appl. Cryst.*, **1976**, 9, 193
- ³⁴ Zyss, J. and Oudar, J. L., *Phys. Rev. A*, **1982**, 26, 2016

- ³⁵ Oudar, J. L. and Zyss, J., *Phys. Rev. A*, **1982**, 26, 2028
- ³⁶ Dougherty J. P. and Kurtz, S. K., *J. Appl. Cryst.*, **1976**, 9, 145
- ³⁷ Webster's Ninth New Collegiate Dictionary, Merriam-Webster Inc., Springfield, **1983**
- ³⁸ Dunwilla, D. D., Carroll, L. B., and Berglund, K. A., *J. Cryst. Growth*, **1994**, 137, 561
- ³⁹ Chakraborty, R., and Berglund, K. A., *J. Cryst. Growth*, **1992**, 125, 81
- ⁴⁰ Cerreta, M. K. and Berglund, K. A., *J. Cryst. Growth*, **1990**, 102, 869-876
- ⁴¹ Chrisman, R. W., McLachlan, R. D., and Harner, R. S., US Patent # 4,672,218, **1997**
- ⁴² Bennett, R. C., Handbook of Industrial Crystallization, Edt. Myerson, A. S, Butterworth-Heinemann, Boston, **1993**

Chapter 1

USING RAMAN SPECTROSCOPY FOR MONITORING POTASSIUM DIHYDROGEN PHOSPHATE BATCH CRYSTALLIZATION

Raman spectroscopy is a useful method for monitoring batch crystallization.

Practical monitoring of an industrial process, such as crystallization, requires the measurements be *in-situ*, done in real time, and are nonintrusive to the process. The measurement needs to be easy to obtain where no special sample preparation is necessary which would introduce error and delay the results. Recent advances in Raman instrumentation enable the *in situ* study of crystallizing systems while meeting the aforementioned requirements. These developments include the use of transmission gratings, the availability of high quality notch filters, and sensitive CCD cameras.

1.1 BACKGROUND

Raman spectroscopy is an optical technique that relies on inelastic light scattering from molecules. The resultant spectra are a measure of the polarizable vibrational energies of the particular molecules involved. Additional information discussing the theory and practice of using Raman spectroscopy can be found elsewhere.¹ The other major topic of this work is crystallization, which is the separation of crystalline material from a solution of that particular species. Here again the theories and principles of the process can be found in the introduction and in greater detail elsewhere.²

The application of this technique is demonstrated on potassium dihydrogen phosphate (KDP). Previous work has been done within the research group³ and elsewhere^{4,5,6,7} on understanding the growth kinetics of dihydrogen orthophosphates. This work demonstrates the ability to monitor the KDP crystallization using Raman spectroscopy. The system can be monitored in real-time, *in situ*, and without perturbation.

1.2 EXPERIMENTAL

The experimental set-up is illustrated in figure 1.1. The key features in monitoring the crystallization are the instrument used and the crystallizer. The instrument permitted rapid and sensitive spectra collection and the batch crystallizer is laboratory scale with a sighting window.

The crux of this work is the spectrometer that was used. Manufactured by Kaiser Optical (Ann Arbor, MI) the HoloLab 1000 uses a 30 milliwatt HeNe laser, a 7 fiber (1 excite, 6 collection) fiber optic probe, and a holographic transmission grating. The resolution is approximately 8 cm^{-1} and the focal length of the probe optic is 6 inches.

The crystallizer is a laboratory scale (400 mL) water-jacketed glass reactor vessel. The optical window is 3 cm in diameter. A marine style impeller provided the agitation of the solution of Aldrich ACS grade KDP which was 30% wt/wt in in-house reverse osmosis water. The crystallizations were done isothermally at 30°C with 1 second exposure time for 25 scans.

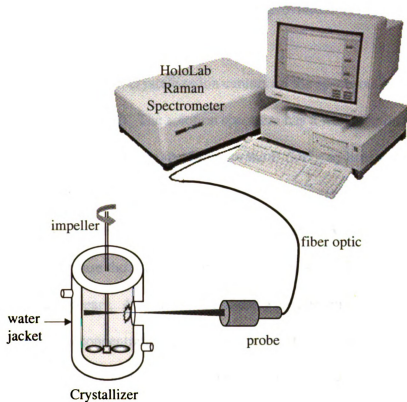


Figure 1.1

The experimental set-up including the Kaiser Optical HoloLab 1000 Raman Spectrophotometer and laboratory scale crystallizer.

1.3 RESULTS AND DISCUSSION

KDP was chosen as an example system because of prior knowledge of its Raman spectrum.³ By using the differences in the crystalline and solution Raman spectra a collection of the changing peaks can be ratioed. This provides a measure of the crystallization process as it occurs.

The monitoring of KDP crystallization centers on the spectra of both the crystal and solution phases (figure 1.2). The solution spectrum has a water band around 3400 cm^{-1} . Two prominent features in this spectrum are the $\text{P}(\text{OH})_2$ symmetric stretch at 886 cm^{-1} and the $\text{O}=\text{P}=\text{O}$ symmetric stretch at 1086 cm^{-1} . The interesting feature of the crystal spectrum is the $\text{P}(\text{OH})_2$ symmetric stretch at 917 cm^{-1} . When going from solution to crystalline phase the $\text{P}(\text{OH})_2$ symmetric stretch shifts 31 cm^{-1} and the $\text{O}=\text{P}=\text{O}$ symmetric stretch disappears. A combination of these changes provides a tool to monitor the decrease in solution concentration and an increase in the presence of crystals. The increasing crystalline peak and decreasing solution peak are illustrated in figure 1.3. Shown is the region centering on the peaks discussed above. The spectra are plotted along a time axis of approximately 5 minute intervals.

By ratioing the solution KDP peak at 886 cm^{-1} and the crystalline peak at 917 cm^{-1} a plot is constructed. The ratio of these peaks as a function of the crystallization time produces a "fingerprint" of that particular batch. This "fingerprint" measures the induction time, rate of concentration decrease, the rate of crystal formation, and the ending point of the crystallization. Additionally, Raman spectroscopy can measure both

the solution phase and crystal phase. Providing a means for monitoring the solution concentration, while simultaneously collecting information about the crystals forming.

The discussion would not be complete without considering the limitations of using Raman for monitoring crystallization. The dominant limit is the particular crystal system and its ability to Raman scatter. The Raman spectrum of the crystallizing species needs to be clear of solvent Raman scatter and have a high enough efficiency. A way to circumvent this would be using resonance Raman and employing chemometric data analysis. In comparison to the SHG technique for monitoring induction time, Raman spectroscopy is expected to be less efficient. As will be demonstrated in the next chapter, SHG has a lower detection limit than Rayleigh scattering. Therefore, SHG would be expected to have lower detection limits than Raman spectroscopy too.

Raman spectroscopy can be used to monitor KDP crystallization. Ratioing the intensity of the solvated molecule and crystalline molecule provides a “fingerprint” of the particular batch crystallization. This “fingerprint” contains the induction time, relative concentration, solid characteristics, and an ending point of the batch crystallization being monitored.

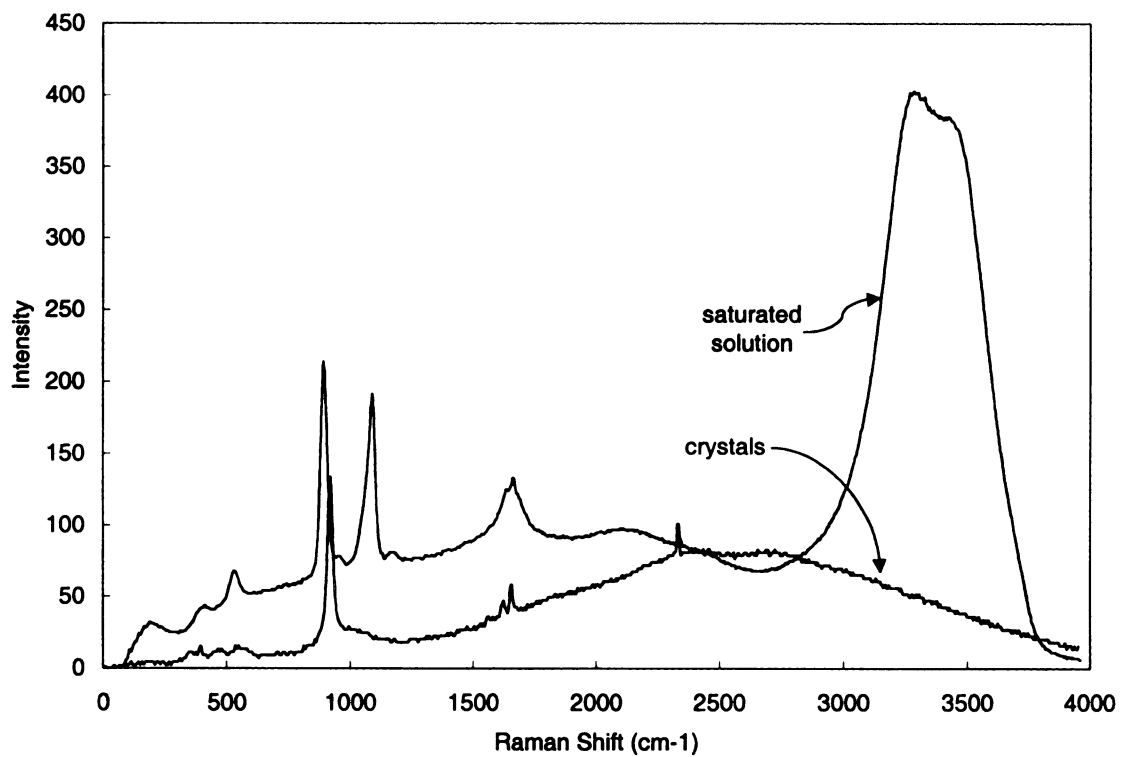


Figure 1.2

Raman spectra of KDP in crystalline and saturated solution taken using the instrument in figure 1.1.

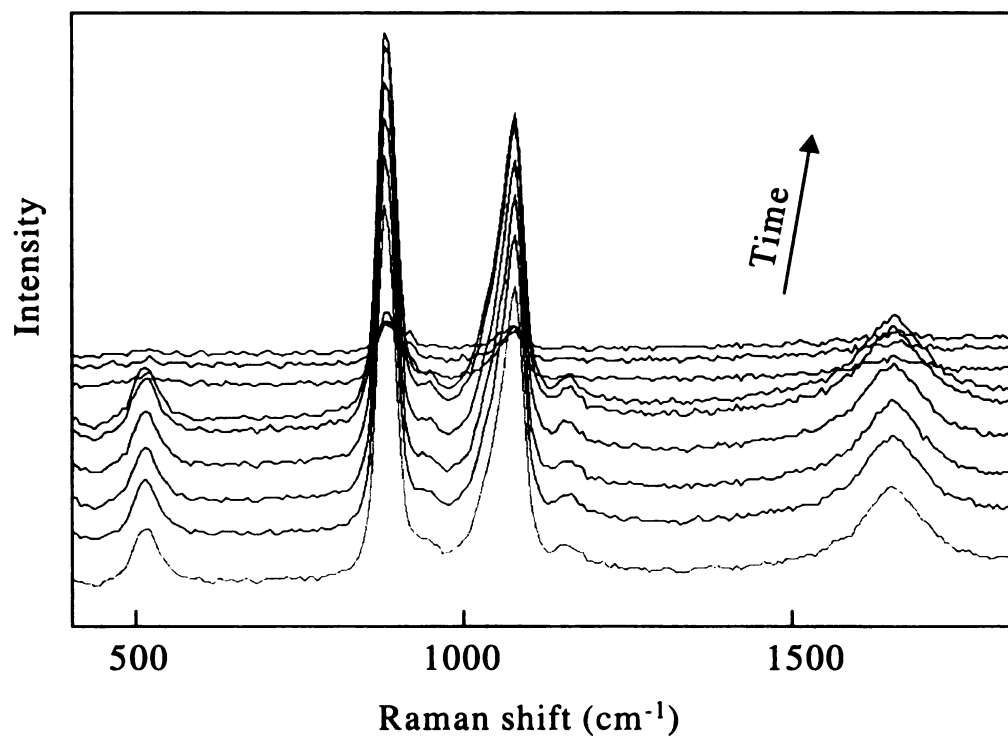


Figure 1.3

Stacked plot of Raman spectra for the KDP crystallization. The spectra are taken at 5 minute intervals starting in the front.

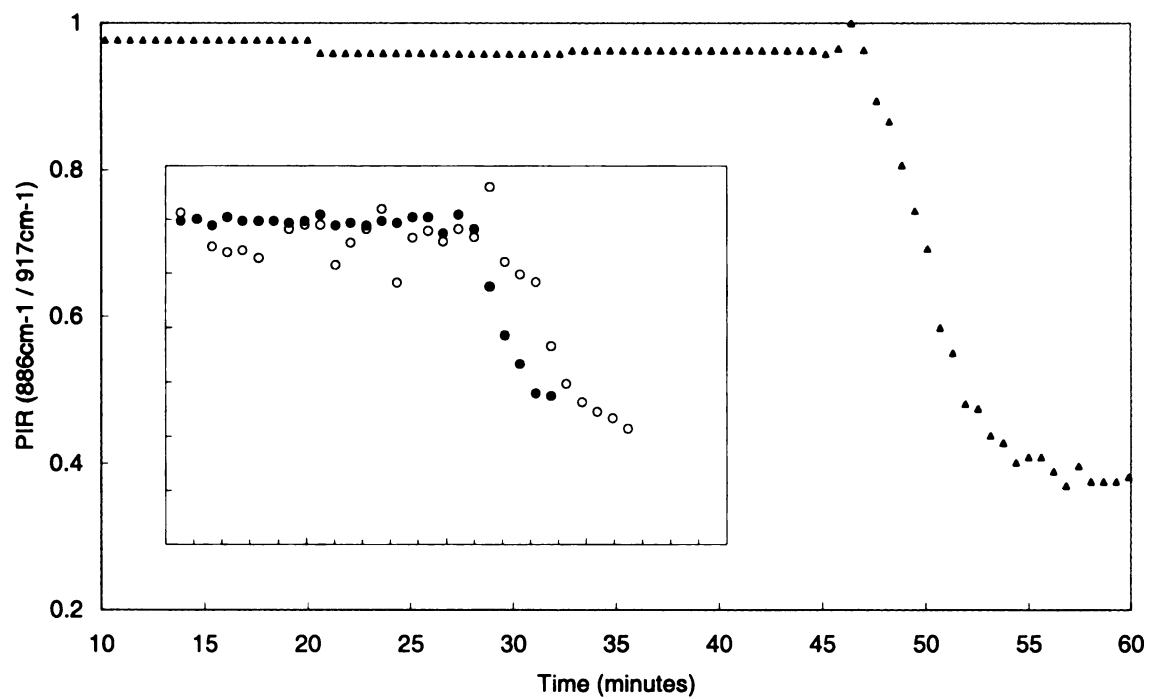


Figure 1.4

Peak intensity ratio of the solution KDP peak at 886 cm^{-1} and the crystalline peak at 917 cm^{-1} . Inset shows repetitive runs of KDP crystallization.

1.4 REFERENCES

¹ Colthup, C. P., Daly, L. H., and Wiberley, S. E., Introduction to Infrared and Raman Spectroscopy Third Edition, Academic Press, San Diego, **1990**

² Mullin, J. W., Crystallization 3rd Edition, Butterworth-Heinemann, Oxford, **1993**

³ Cerreta, M. K. and Berglund, K. A., "The Structure of Aqueous Solutions of Some Dihydrogen Orthophosphates by Laser Raman Spectroscopy", J. Cryst. Growth, **1987**, 84, 577

⁴ Van Enckevort, W. J. P., Rosmalen, R. J., and Van Der Linden, W. H., *J. Cryst. Growth*, **1980**, 49, 502

⁵ Barata, P. A. and Serrano, M. L., *J. Cryst. Growth*, **1996**, 160, 361

⁶ Mullin, J. W. and Amatavivadhana, A., *J. Appl. Chem.*, **1967**, 17, 151

⁷ Paul, B. K. and Joshi, M. S., *Ind. J. Pure & Appl Phys.*, **1976**, 14, 544

Chapter 2

THE APPLICABILITY OF SECOND HARMONIC GENERATION FOR *IN SITU* MEASUREMENT OF INDUCTION TIME OF SELECTED CRYSTALLIZATION SYSTEMS

Second Harmonic Generation (SHG) is proposed for measuring crystal formation in supersaturated solutions. SHG is able to detect some crystalline material in a liquid medium. The focus of this paper is to describe the *in situ* and noninvasive technique for measuring the induction time of batch crystallization process as using SHG.¹

2.1 BACKGROUND

Crystallization is the formation of crystalline material (solid phase) from solution (liquid phase). Crystallization is composed of nucleation and crystal growth. The chemical potential of a supersaturated solution is the driving force, where a small supersaturation favors growth and a large supersaturation favors nucleation. The optimal crystallization is to have an appropriate number of nuclei present to permit crystal growth. The relationship between these two processes is much more complex and a detailed description appears elsewhere.¹ The two common methods for introducing nuclei in an industrial batch crystallizer are to either seed the supersaturated solution or

¹ This chapter was adapted from previously published work; LeCaptain, D. J. and Berglund, K. A., *J. of Cryst. Growth*, 203, 1999, 561

increase the supersaturation to cause self-nucleation. Seeding is favorable because of the lower supersaturation required, therefore favoring growth and ultimately larger mean crystal sizes. The drawbacks of seeding are that an additional step is necessary and guaranteeing the crystal seed quality is necessary. Conversely, a large supersaturation is necessary to cause self-nucleation, but this large chemical potential increase the effect of system parameters such as crystallizer shape, agitation, temperature variations, etc., has on the nucleation. Significant batch variations result, making it very difficult to predict the nucleation.²

Nucleation is the formation of crystalline species from a supersaturated solution. The time from a supersaturation level to formation of the first nuclei is the true induction time. The experimental or measured induction time is the true induction time plus the time necessary for the crystals to grow to a detectable size. Therefore the method of detection plays an important role in the induction time measured.³ The more sensitive the technique the closer to the measured time is to the true induction time. Additionally, nucleation is very dependent on the system conditions, therefore induction time is not constant for different batches. The importance of induction time relates back to the previous paragraph on nucleation versus growth. Ultimately the *in situ* measuring of induction time aids in the efficient control of the crystallizer and the better technique would be more sensitive.

Induction time measurements can be done using the non-linear optical technique of SHG. Examples of the previous studies on powders suggest the potential of using SHG for monitoring crystallization.^{4,5,6} Since the advent of lasers, the efficiency of non-centrosymmetric crystals as frequency doublers has been thoroughly studied. A review

of the nonlinear efficiencies, how well a species responds in the second order process, of organic crystals by Oudar and Zyss emphasizes this point.^{7,8} In particular studies of the second harmonic from powders demonstrate the possibility of use in solutions.⁴ SHG is the nonlinear conversion of two photons (frequency ω) to a single photon (frequency 2ω). It is the interaction of the electromagnetic wave dipole and the dipole of the medium. The medium has to have a dipole within the coherence length of the laser pulse for this phenomenon to occur. Nanosecond and shorter laser pulses are required for high energy density, which are necessary for the non-linear response to occur. The key to the process is size and rigidity of the dipole species. Foremost, a dipole is necessary, meaning a centrosymmetric structure. The dipole species also has to be large enough and properly structured to couple with the light wave to produce the second harmonic. The randomness of the bulk solution causes it to be SHG inactive.

The noncentrosymmetric requirement for the SHG process limits the number of crystal systems. It is necessary to have a noncentrosymmetric crystal structure. Large portions of batch crystallizations are performed on pharmaceuticals and fine chemicals, which are generally biological or biologically related molecules. These types of molecules tend to be noncentrosymmetric, producing noncentrosymmetric crystal structures and therefore ideal for SHG detection.

2.2 EXPERIMENTAL

The Experimental set-up is diagrammed in figure 2.1. A Quanta-Ray DCR laser was used to produce an average 12 to 14 millijoules per pulse energy at 1064 nanometers (nm). The pulse width was approximately fifteen nanoseconds at a frequency of 10 Hz.

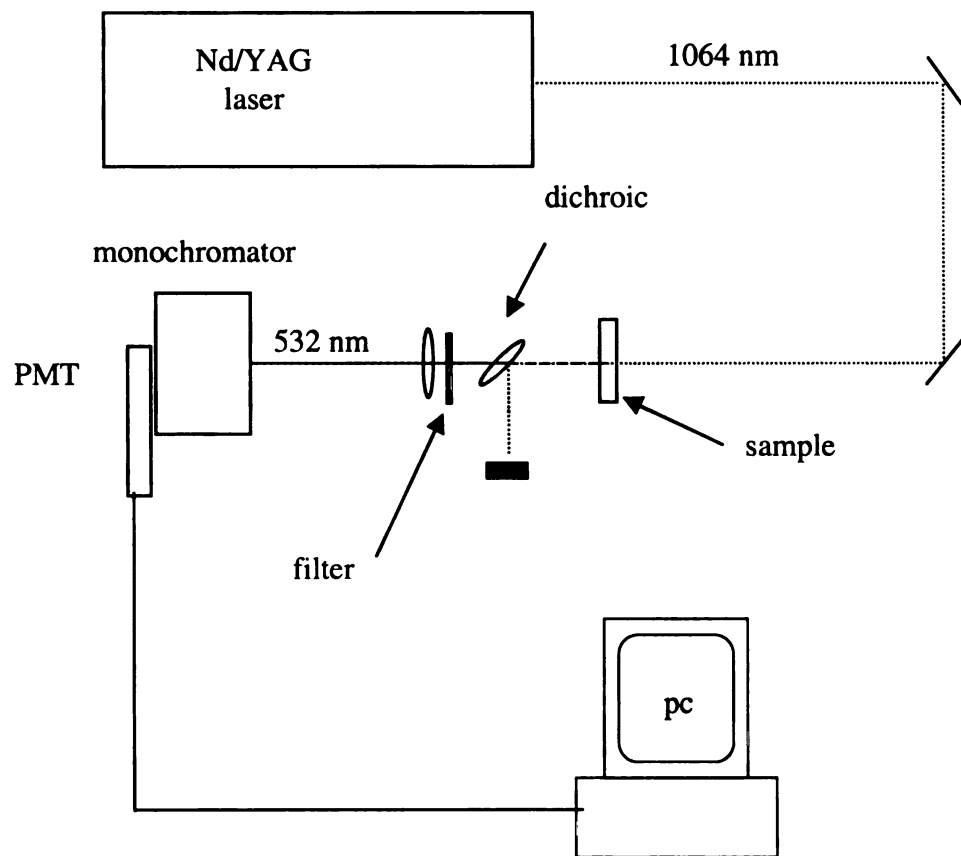


Figure 2.1

Experimental set-up used for the SHG experiments.

The turbidity measurements were done by averaging the transmitted intensity at 490 nm from a Guided Wave fiber optic absorbance instrument.

The crystallizer was designed to mimic an industrial crystallizer with agitation in a forced circular configuration and temperature control to $\pm 0.3^{\circ}\text{C}$ by a NesLab water circulator. A 1-inch-impeller turning at 650 rpm pumped the solution. A high power dichroic mirror and glass filter were used to filter the incident light (1064 nm) from the generated second harmonic light (532 nm). The second harmonic was measured using a Spex monochromator and 1106 Hamamatsu PMT. A SRS Gated Boxcar Averager averaged the collected second harmonic intensity over either 3 to 10 seconds. Collection optics and PMT settings were held constant. The data were collected every 15 to 30 seconds by a short program in National Instruments LabView software.

The potassium dihydrogen phosphate (KDP), potassium chloride (KCl), Citric Acid, chromium chloride (CrCl_3) L-lysine monohydrochloride (lysine m-HCl), and were used as received from Aldrich Chemical Company. KDP was chosen for the majority of the studies because of availability and good second harmonic efficiency. Lysine m-HCl and α lactose were chosen to demonstrate the technique on an amino acid and a soluble organic compound. The solution concentrations were measured by percent mass in water. The water used was the building tap, reverse-osmosis water. The percent supersaturation (σ) was calculated as follows:

$$\sigma = (\text{wt \% of solution} / \text{wt \% @ saturation} - 1) * 100$$

The weight percent saturation was extrapolated from solubility data.²

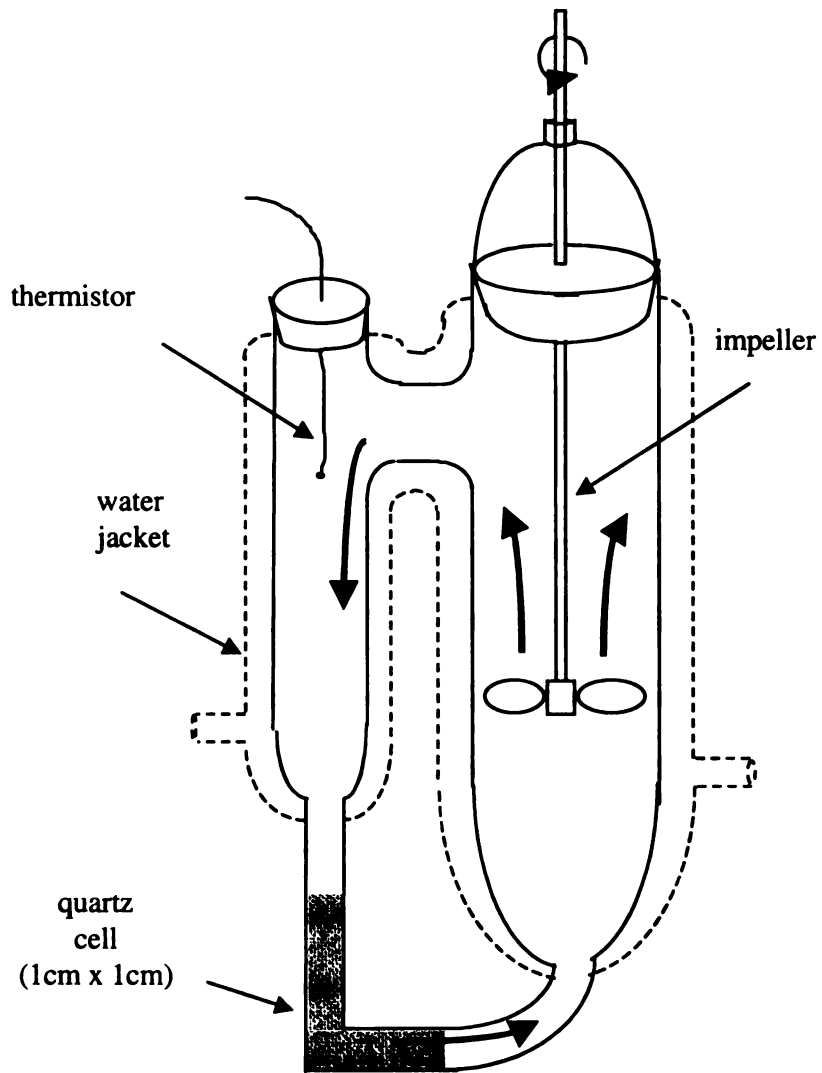


Figure 2.2

Schematic of the experimental batch crystallizer, temperature controlled with solution pumping action. The operating solution volume is 390 mL.

All data collection was performed under isothermal conditions. The samples were weighed and then dissolved in the crystallizer by elevating the temperature to 45°C (above the saturation level) for approximately 1 hour. The solution was cooled at the maximum rate possible taking approximately 3-5 minutes to reach 30.0°C ± 0.2°C which was maintained for the duration of the experiment. The induction time measurement was started when the solution temperature reached 30.1°C. The lysine m-HCl was crystallized by ethanol anti-solvent crystallization.

2.3 RESULTS AND DISCUSSION

This technique can measure the presence of crystals in a liquid medium by detecting the produced second harmonic. Nucleation and growth of the crystals causes the increase in second harmonic light produced. Detection in bulk solution is possible because of the non-centrosymmetric symmetry requirement for SHG. This symmetry requirement also eliminates interference from the bulk solution; foreign particles such as air bubbles or impurities, which are not SHG active. The crystals are the medium necessary for SHG, therefore no probe molecules or special sample treatments are necessary, which could potentially perturb the system. Another advantage of SHG is detection over a dark background, allowing for detection that is more sensitive.

A brief explanation of specific SHG theory indicates why this process works. SHG requires a non-centrosymmetric medium within the coherence length of the incident wavelength, otherwise phase cancellation of the second harmonic will occur. When the particle is larger than the coherence length, surface SHG effects can be measured.⁹ The particle (crystals in this case) are smaller than the coherence length, therefore the second-

order light scattering process called hyper-Rayleigh scattering is a more likely explanation. Hyper-Rayleigh scattering occurs when density and orientation fluctuations of the crystal species in bulk solution disrupt the phase cancellation previously discussed.¹⁰

The crystal formation of KDP monitored using SHG is shown in figure 2.3. The results show the second harmonic intensity increasing from zero baseline (region I) to the normalized full-scale detection limit of the apparatus (region IV). Region II shows the first change in signal. The left is the measured induction time for the process. Region III occurs after formation of adequate surface area (adequate number of nuclei) and is the desupersaturation of the solution. This is shown by the steeply sloped region and is due to a combination of growth and nucleation. Finally, after substantial crystal formation the supersaturation is depleted and the solution reaches its saturation level again (region IV), with no additional crystal growth or nucleation.

The next step in demonstrating this technique is reproduction of the induction time measurement. Figure 2.4 illustrates the induction time measurement of various KDP supersaturation that were isothermally self-nucleated. The induction time is defined here as the change in signal exceeding the 95% confidence of the baseline in the crystal formation curve. Clearly, a mathematically more rigorous method could be employed, but the inherent discrepancies in induction time measurement do not make it necessary at this time. As expected, the measured induction time increases as the percent supersaturation of the solution decreases. The increase in the range of induction times as the percent supersaturation is decreased demonstrates the need for *in situ* monitoring. This variation is expected and parallels similar published data on KDP induction times.¹¹

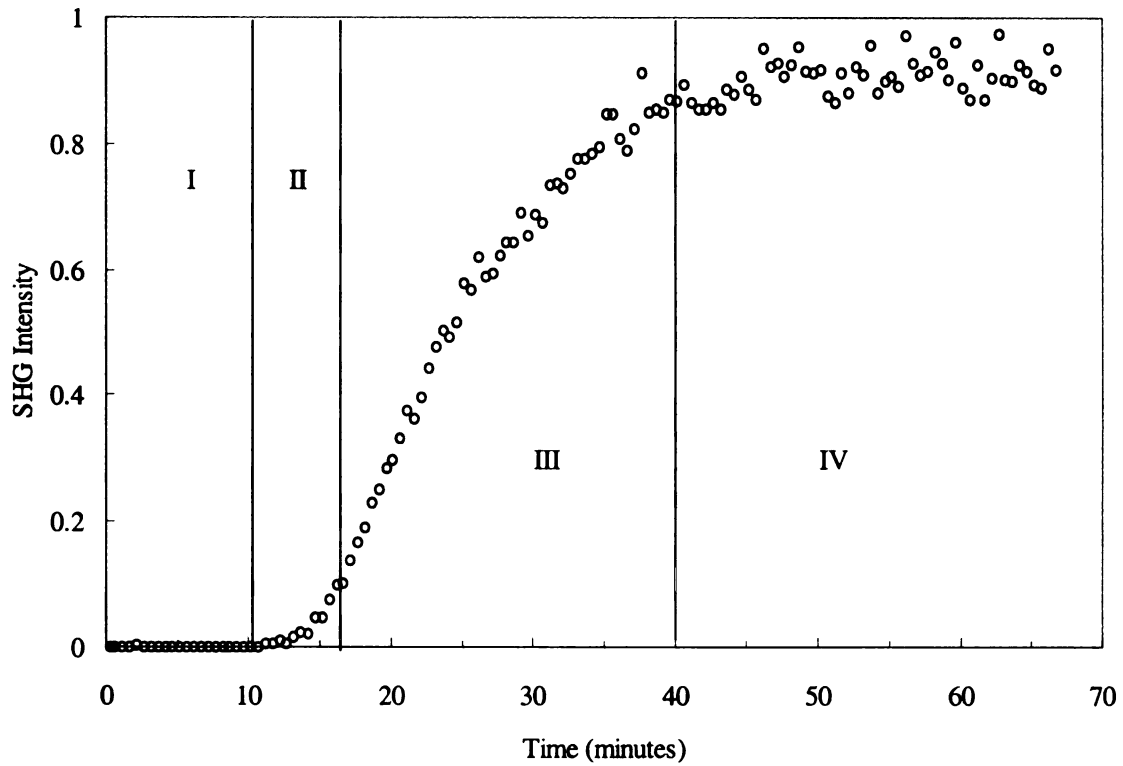


Figure 2.3

Typical Crystal Formation of potassium dihydrogen phosphate (8.9% supersaturated KDP at 30 °C).

Region I: Supersaturated solution, no crystals

Region II: Self-nucleation, crystals starting to form (induction time)

Region III: Rapid desupersaturation, nucleation and crystal growth

Region IV: Return to saturation, no more nucleation or growth

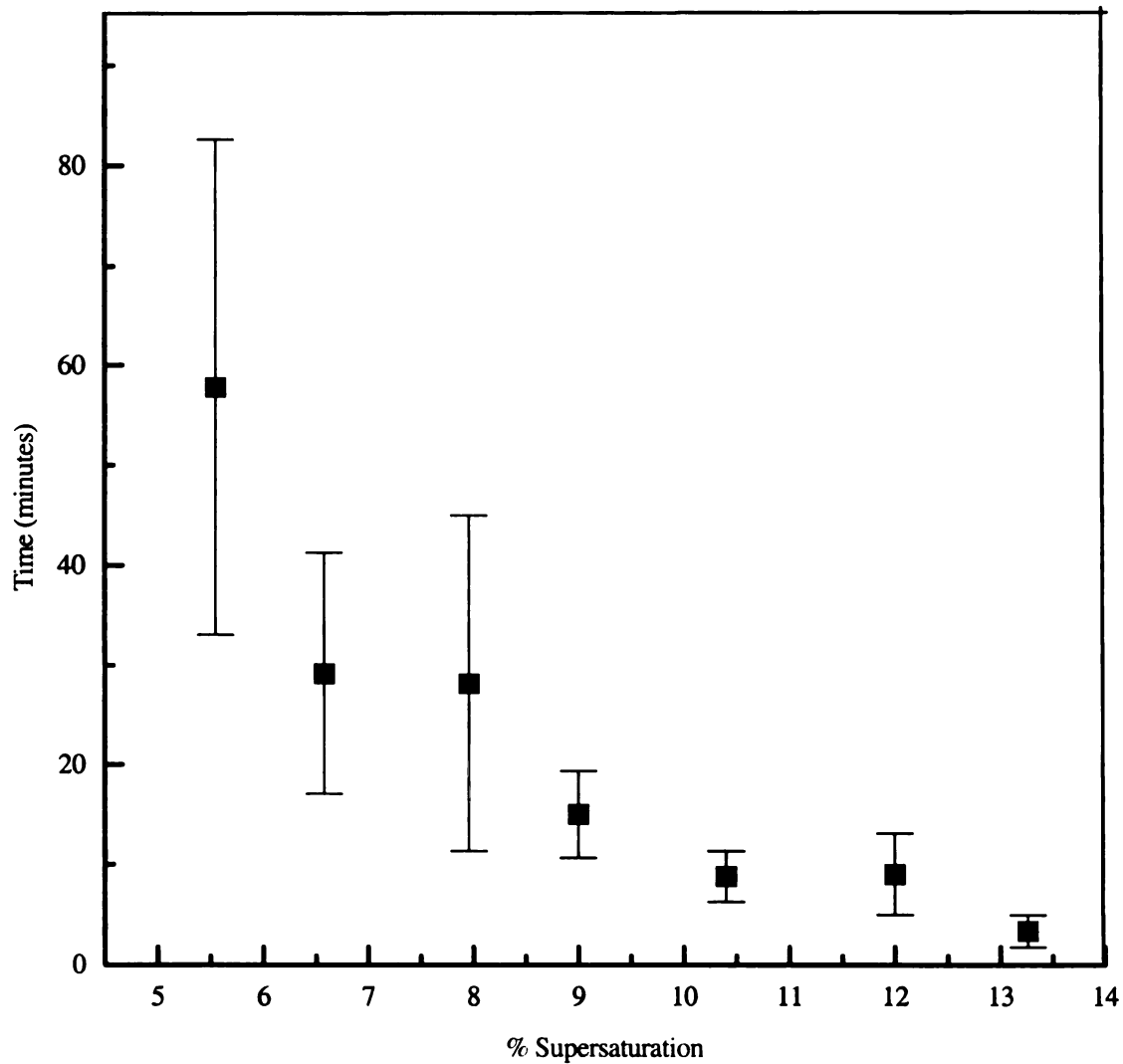


Figure 2.4

Isothermal induction times for varying concentrations of KDP super saturated solutions. (% Supersaturated is the wt % over the saturation value.) All measurements were done at 29.7°C with the same 5-minute cool down to supersaturation level.

A concern of this technique that needs to be addressed is the effect of the laser light used. A second harmonic intensity from a saturated solution containing crystals was measured by varying the laser power from complete signal attenuation (0.9 mJ/pulse) to the threshold of the filtering optics (1.5 mJ/pulse). The change in signal varied linearly with the measured signal through this limited range that is well below the energy used in the laser crystal induction studies cited above. Additionally at high laser light energies perturbation of the system could be a concern. Garetz and coworkers have demonstrated static urea crystal nucleation induced by laser light.¹² Coinciding with this would be sample degradation. To address this concern KDP crystallization was run under twice the laser energy used for the measurements and no perturbation of the system was observed. This can be justified by the large sampling volume used and the motion of the solution. The combination of those two negates the concerns of localized heat build up or sample degradation.

Additional crystal systems were studied to demonstrate the versatility of this technique. Figure 2.5 and 2.6 are the SHG measurements of α lactose and lysine m-HCl respectively. Lactose a very soluble organic material, lysine an amino acid, and KDP an inorganic salt are a sampling of the range of materials this technique can be used for. Note as the lactose is crystallizing a maximum intensity is reached and then begins to decrease. This is due to the large amount of crystalline material that scatters both the incident laser beam and SHG produced. SHG (O) and light scatter (X) monitoring of lysine m-HCl. The SHG is normalized to the amount of SHG detected, whereas the light scatter is the amount scattered with the saturated solution being the zero measure. The data shown is 200 g. lysine m-HCl dissolved into 300 g. water, and then cooled to 20 °C.

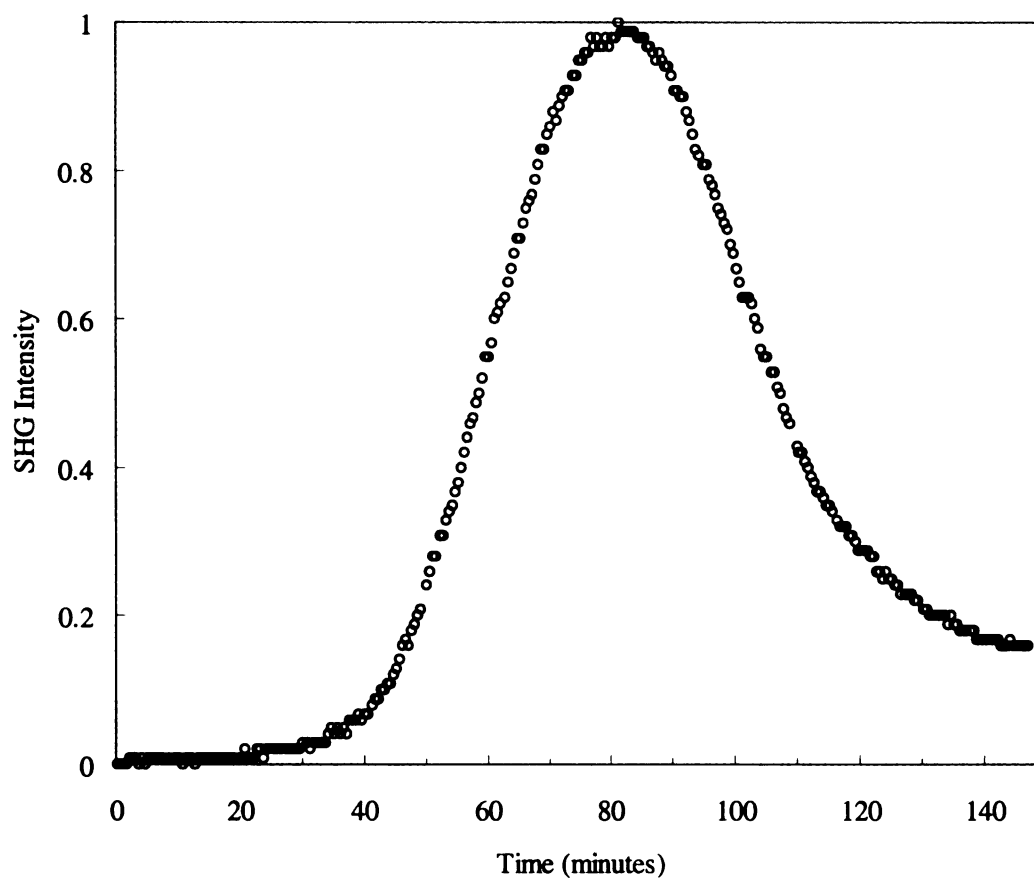


Figure 2.5

SHG monitoring of 35.4% supersaturation α -Lactose crystal formation. The crystallization was performed isothermally at 20 °C. The maximum and subsequent decrease in measured intensity is due to scatter from the large quantity of crystals.

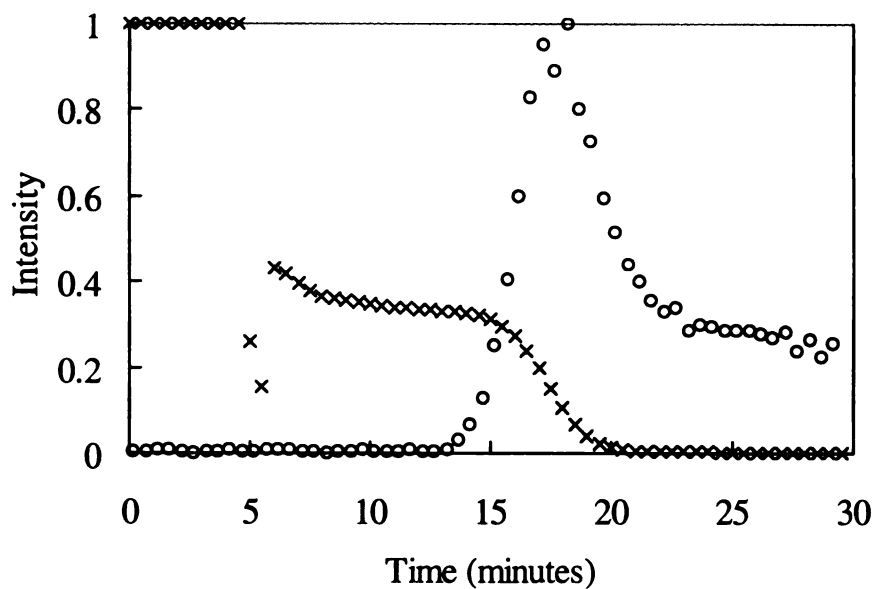


Figure 2.6

SHG(O) and light scatter(X) monitoring of L-lysine-HCl. The SHG is normalized to the amount of SHG detected, whereas the light scatter is the amount scattered with the saturated solution being the zero measure. The data shown is 200g lysine m-HCl dissolved into 300g water, and then cooled to 20 oC. The addition of 30 mL of ethanol occurs at the 5-minute mark.

The addition of 30 ml. of ethanol occurs at the 5-minute mark. It can be seen that a large amount of light is scattered due to the intermixed phases of concentrated water and the fresh ethanol, but no crystalline species are present until approximately 7 minutes later.

An area to be addressed is the lack of symmetry present at crystal to solution interfaces. To demonstrate that SHG is not produced by the solid to liquid phase separation and is indeed only the crystal the crystallization of KCl and citric acid were monitored. Both have centrosymmetric crystal structures that won't produce the second harmonic. Since no second harmonic was observed, it is concluded that the boundary region also does not produce the second harmonic.

The final area studied with this technique is in comparing it to light scattering measurements. SHG and light scatter were simultaneously used to monitor KDP crystallization. The light scatter instrumentation is described previously and measures percent transmittance. By subtracting the percent transmitted from 100% T of the under saturated solution the percent of light scattered is obtained and this is what is plotted. Figure 2.7 shows the KDP crystallization curve being monitored by both techniques. It appears the techniques are very comparable, but the increased sensitivity available from the SHG apparatus can be seen in Figure 2.8. By expanding the axis and looking at the induction time, it is apparent that the SHG is more sensitive to the crystals forming. Therefore, the SHG method measures a shorter induction time.

2.4 CONCLUSIONS

Second harmonic generation is demonstrated as a technique for monitoring crystal formation in supersaturated solutions. This method is advantageous over turbidometric

methods as it able to measure the crystal formation *in situ* and shows a more sensitive response. The availability of laser systems and advances in laser design make this method viable for numerous industrial applications.

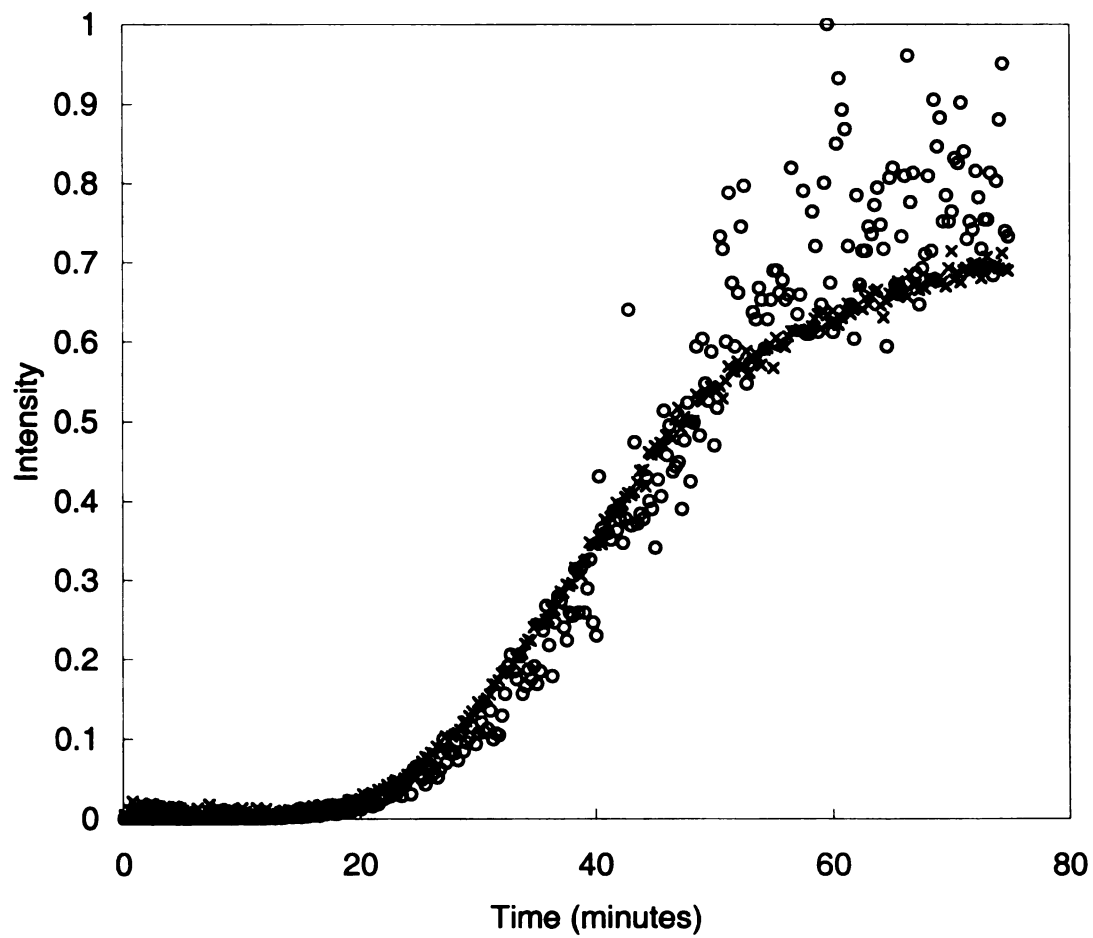


Figure 2.7

Comparison of the induction time measurement using SHG (O) and light scatter (X) on crystallization curve of 7.53% supersaturated solution of KDP.

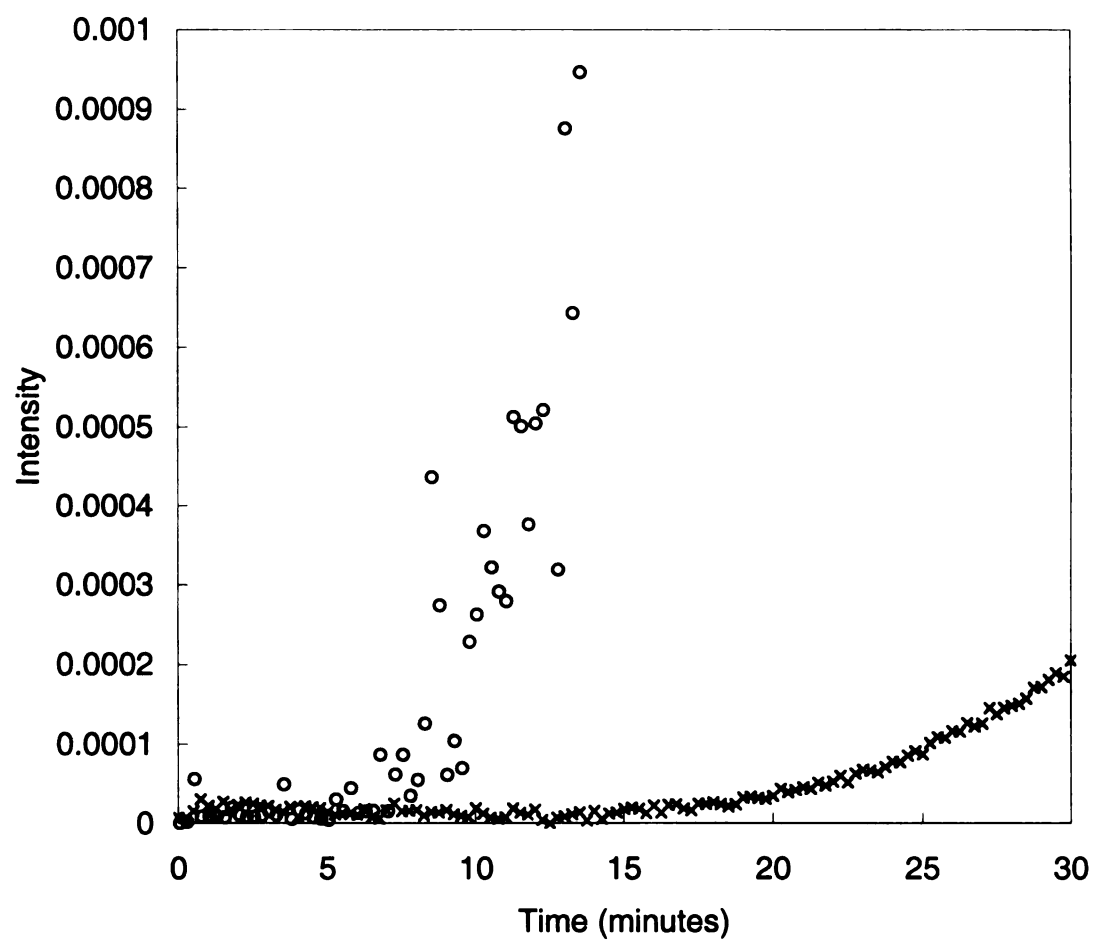


Figure 2.8

The early time frame expanded from figure 2.7. The intensity change for SHG is much greater than the light scattering and the SHG has an earlier detection of the induction time.

2.5 REFERENCES

- ¹ Berglund, K. A., Edited Myerson, A. S., Handbook of Industrial Crystallization, Butterworth-Heinemann, Boston, **1993**, 89-101
- ² Mullin, J. W., Crystallization, Butterworth-Heinemann, **1993**
- ³ Otakar, S. and Mullin, J. W., *J. Coll. Int. Science*, **1988**, 123, 43
- ⁴ Kurtz, S. K. and Perry, T. T., *J. of Appl. Phys.*, **1968**, 39, 3798
- ⁵ Dougherty, J. P. and Kurtz, S. K., *J. Appl. Cryst.*, **1976**, 9, 145
- ⁶ Coda, A. and Pandarese, F., *J. Appl. Cryst.*, **1976**, 9, 193
- ⁷ Zyss, J. and Oudar, J. L., *Phys. Rev. A*, **1982**, 26, 2016
- ⁸ Oudar, J. L. and Zyss, J., *Phys. Rev. A*, **1982**, 26, 2028
- ⁹ Wang, H., Yan, E. C. Y., Borguet, E., and Eisenthal, K. B., *Chem. Phys. Lett.*, **1996**, 259, 15
- ¹⁰ Terhune, R. W., Maker, P. D., and Savage, C. M., *Phys. Rev. Lett.*, **1963**, 14, 681; Clays, K. and Parsoons, A., *Phys. Rev. Lett.*, **1991**, 66, 2980
- ¹¹ Barata, P. A. and Serrano, M. L., *J. Cryst. Growth*, **1996**, 160, 361
- ¹² Garetz B. A., Aber, J. E., Goddard, R. G., Young, R. G., and Myerson, A. S., *Phys. Rev. Lett.* **1996**, 77, 3457

Chapter 3

AN *IN SITU* SECOND HARMONIC GENERATION PROBE FOR MONITORING AND CONTROLLING BATCH CRYSTALLIZATION

The probe for measurement of SHG is described for immersion into a crystallizer. The demonstration of the SHG technique for monitoring crystal formation appears in the previous chapter and elsewhere.¹ The present work demonstrates that the SHG probe can be used *in-situ* and in real time during crystallization, thus enabling control to be exercised. The probe is described in detail and control of L-lysine-monohydrochloride (Lmhc) crystallization is presented.

3.1 SYSTEM DESIGN

The SHG probe described is designed for *in situ*, real time measurements. The system was constructed from standard modules and equipment to demonstrate the feasibility of the technique and the system.

A schematic of the system is shown in figure 3.1. A Coherent Infinity Laser produces the incident beam (1064 nm). The pulses are approximately 4-6 ns wide at a repetition rate of 25 pulses per second. The pulse energy was measured to be 2 to 3 millijoules in front of the probe. Second harmonic light detection is accomplished using a Heath Photomultiplier Module, model EU-701-30. The PMT voltage was 900V and

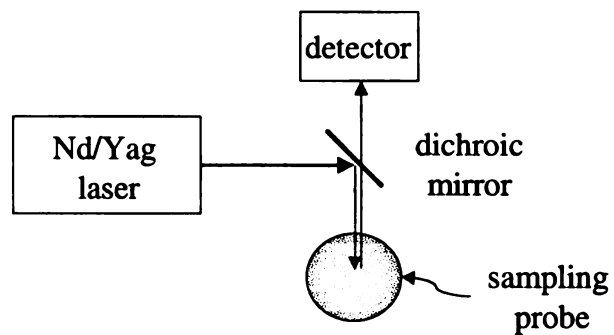


Figure 3.1

General schematic shows the experimental design. A pulsed laser provides the incident 1064 nm lights measured using a PMT. The sampling probe is detailed in figure 3.2.

was sampled with a SRS BoxCar Averager. Each datum is the back weighted average of 100 laser pulses. The average PMT output signal is transferred to LabView software on a PC where the intensity is stored and plotted versus the time from experiment start.

The probe design enables SHG measurements to be made in a batch crystallizer. Figure 3.2 is a diagram of the probe and how it operates in a crystallizer. The 400 mL crystallizer has a water jacket for $\pm 0.3^{\circ}\text{C}$ temperature control by a NesLab water circulator. The laboratory scale crystallizer uses a 1-inch marine style impeller turning at 650 rpm for agitation. The SHG probe transmits the 1064 nm incident light into the sample and separates the generated second harmonic (532 nm) from the incident for transmission to the PMT. The high power dichroic mirror reflects the incident laser beam into the glass waveguide (1cm x 15 cm glass rod). The dichroic mirror is reflective to 1064 nm light, but transmissive to 532 nm light. The glass waveguide channels the incident laser beam into the bulk of the solution, avoiding the surface or edges of the crystallizer where perturbations or inconsistencies tend to occur. The path length or area being sampled is the distance between the end of the waveguide and hypotenuse of the leg-mirrored prism. The incident beam (1064 nm) and the majority of the generated second harmonic (532 nm) are co-linear, therefore are reflected by the mirrored prism. The legs of the reflecting prism are mirrored because the similarities in refractive index of the solution and the glass prism prevent efficient reflection using a regular prism. Additionally, the mirrored surfaces of the prism are not exposed to the solution, which prevents scratching. Transmissivity differences of the solutions can be accounted for by adjusting the path length. The glass waveguide transmits the generated second harmonic either reflected from the first pass through the solution or upon the second pass to the

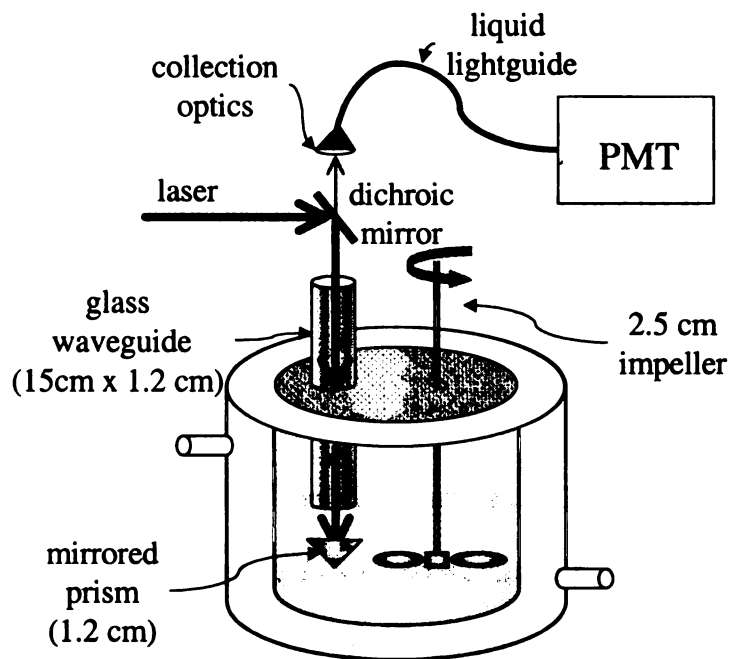


Figure 3.2

Laboratory scale (~400mL) crystallizer that has the SHG probe immersed to show the details of the design. The system design section describes the components in detail.

dichroic mirror. The dichroic mirror transmits the 532nm light and reflects the residual incident beam (1064 nm) into a beam dump. The transmitted second harmonic light is focused into an Oriel Liquid Light Guide and transmitted to the PMT. The separation efficiency of the second harmonic from the incident by the dichroic mirror is not 100% but the residual 1064 nm light is filtered by the liquid light guide. The liquid light guide is very efficient in the transmission of 532 nm light and very inefficient for the 1064 nm light. The light guide has a large acceptance angle allowing for easy alignment and flexibility similar to fiber optic cable allowing for versatility.

3.2 APPLICATION

The design and ultimately the application of the SHG probe encompasses crystal systems that lack inversion symmetry. Pharmaceuticals and fine chemicals tend to be chiral and complex molecules that in turn tend to form crystals that meet this symmetry requirement. The potential of the technique can be realized by considering the numerous crystal species that have been quantitatively determined in powder form.^{2,3} The main consideration is whether the SHG efficiency of a particular species is great enough to be measured. The refractive index of the crystal and solution at both the incident wavelength and second harmonic wavelength determine the efficiency of the second harmonic. From a practical point of view the testing of each crystal system will likely prove the easiest and most reliable way to determine the viability of the SHG probe. The SHG probe described above works for α lactose, potassium dihydrogen phosphate, urea, d-Sorbitol, and L-glutamic acid, but this by no means is an inclusive list. The SHG powder efficiency of these molecules is in the relative magnitude of KDP as previously

reported.³ The crystallization of these molecules is not shown, rather are mentioned to emphasize the broader applications possible.

By monitoring the Lmhc (L lysine monohydrochloride) crystallization the mean crystal size and the size distribution can be improved. A Lmhc solution was cooled in an uncontrolled manner ($\sim 2^{\circ}\text{C} / \text{min.}$) to serve as a reference to the controlled experiments. The controlled crystallization was done the same except the cooling was changed in response to the presence of crystals. Obtaining larger crystals requires favoring crystal growth over nucleation, thus a low supersaturation is desired. Growth cannot occur without first some crystal nucleation, but nucleation needs a high supersaturation. Therefore as soon as crystals are present stopping the increase in supersaturation (stop the cooling) will allow more crystal growth and less nucleation.

The similarities for the two experiments consisted of dissolving 80 grams of Lmhc into a mixed solvent of 150 mL water and 100 mL ethanol. The solution was heated to 80°C and then rapidly cooled to 50°C where the time was started. For the reference experiments the cooling was continued until the temp reached 5°C . The cooling rate was approximately 2 degrees centigrade per minute. The slurry was filtered, dried, and sieved. The filtering, drying and sieving methods remained constant for all samples analyzed. The filtering consisted of Whatman number 2 paper in a Buchner funnel. The crystals were rinsed with cold ethanol and allowed to dry in room conditions for 24 hours. The sieves were standard Fisher Brand Scientific 8 inch sieves, mesh numbers 16, 25, 30, 35, 40, 45, 60, and 80 with a sieving time of 25 minutes.

The controlled experiments were cooled until evidence of crystal formation appeared in the SHG at which point the cooling was stopped. Because of signal to noise

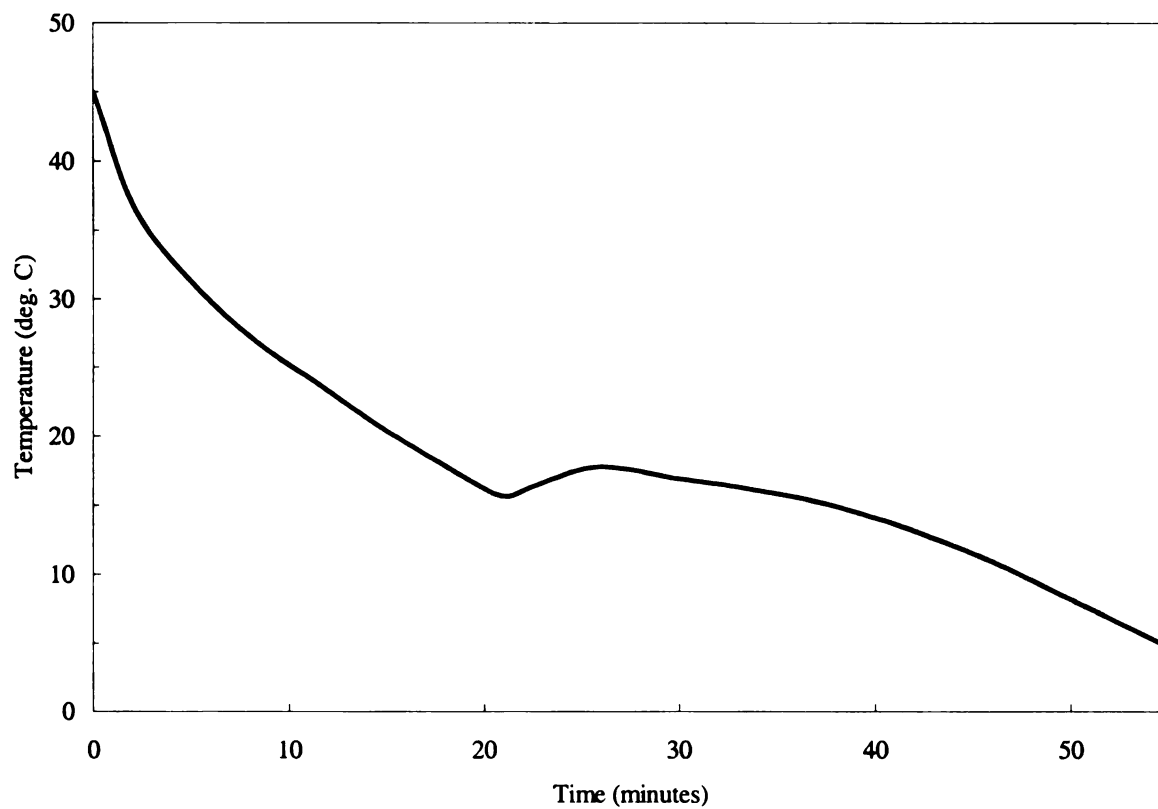


Figure 3.3

Cooling curve for L-lysine monohydrochloride controlled crystallization shown in figure 3.4. The control occurs at 21 minutes when the cooling is stopped in response to crystal detection.

considerations an approximate 20% increase in the SHG signal was the criteria used for determining the presence of crystals. Figure 3.4 shows a typical cooling curve. A slight temperature elevation occurs due to the heat of crystallization. After stabilization of the SHG signal occurred cooling was again started and continued to 5°C when the slurry was filtered, dried, and sieved. The SHG data are shown in figure 3.5. Note the appearance of the second harmonic at 22 minutes, which corresponds to the point when cooling was halted and the temperature slightly increased. The large quantity of crystalline material present after nucleation causes the SHG photons to be scattered and the SHG signal lost. The preceding procedure was repeated and used for obtaining the crystal size distribution data shown in figure 3.5. The population distribution is calculated from the following equation.⁴

$$N = W / (k_v * \rho * L^3)$$

Where N is the number of crystals, W the mass of crystals, k_v is the volume shape factor, ρ is the density, and L is the average crystal size. The volume shape factor approximation for a sphere or cube is 6.⁵ The average size between the upper and lower sieves of a tray approximates the crystal size for that tray. Figure 3.6 shows the crystal size distribution for the controlled and reference crystallizations of Lmhc. Note, the controlled and reference crystal mean size data points are offset for clarity of the figure. The controlled experiments (square) have a slightly larger mean crystal size (316 microns versus 303 microns) than the reference (x) experiments. Also, the deviation for each size is smaller for the controlled crystallizations.

Visual inspection of the crystals shows the importance of the control of the crystallization. Figure 3.7 is a photograph of the crystals produced in the controlled

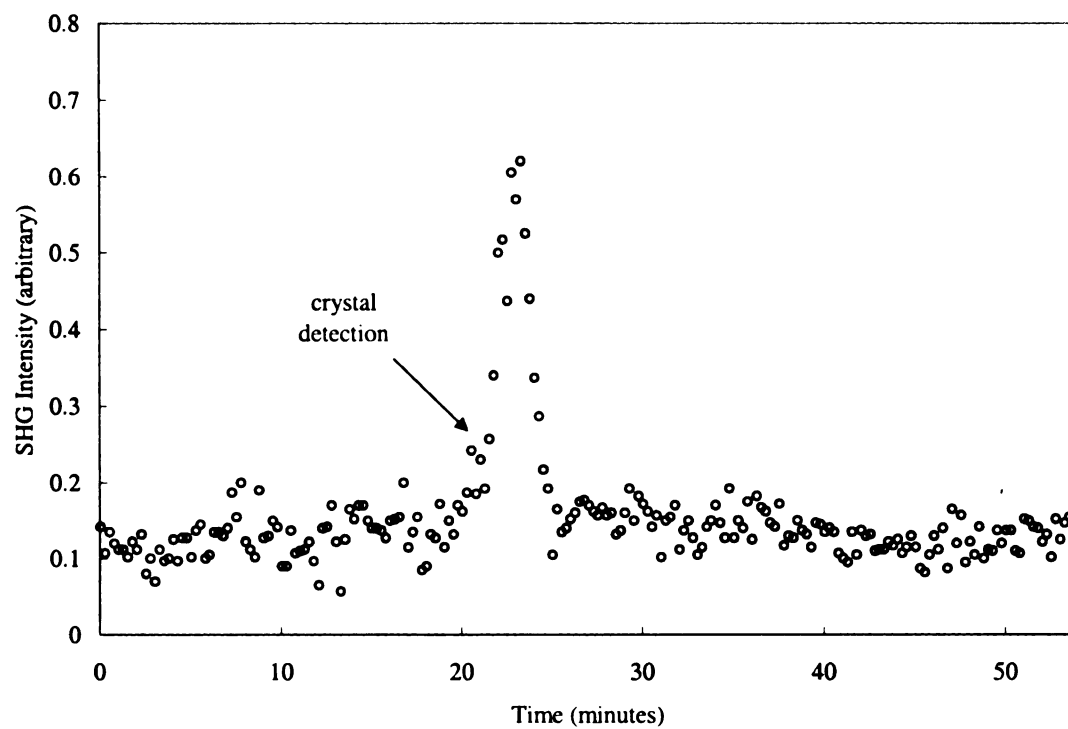


Figure 3.4

SHG output from a typical L-lysine monohydrochloride crystallization.
Cooling crystallization of 80 g in 150 mL water / 100 mL ethanol solution.
The cooling profile is shown in figure 3.4.

experiments and figure 3.8 is a photograph of the reference experiment. The samples photographed were collected from corresponding sieve sizes (#45 mesh number) and handled as described above. Controlling the crystallization produces crystals with a uniform shape. The reference, uncontrolled, experiment photo shows a mix of crystals and agglomerates (figure 3.7). Recalling that agglomerates are assemblies of smaller crystals the results of the size distribution need to be interpreted differently. The reference experiments have a represented larger mean size than actually exists because of the agglomerates. The lack in crystal uniformity will be more evident when the agglomerates easily break down with handling.

The relative efficiency of this configuration versus the previously described system (Chapter 2) needs to be addressed. Experimentally the probe is more versatile. The optical path is not interfered with when samples are changed, but the additional optics necessary cause an estimated 25% decrease in the second harmonic collection. Modifications to the probe would permit a more efficient, robust, flexible, and cost effective device. In replacement of the glass waveguide that is submerged into the solution a bifurcated fiber optic could be employed to transmit the incident 1064 and then collect the generated 532 nm light. Focusing optics would need to be incorporated at the end of the fiber bundle. Either a PMT or a high speed photodiode could handle measurement of the generated second harmonic. Practical consideration of the laser indicates that the research grade laser used here exceeds the requirements for the probe. A lower power, air cooled laser would be more economically feasible and convenient. Thus, the entire apparatus could be substantially reduced in size and increased in rigidity.

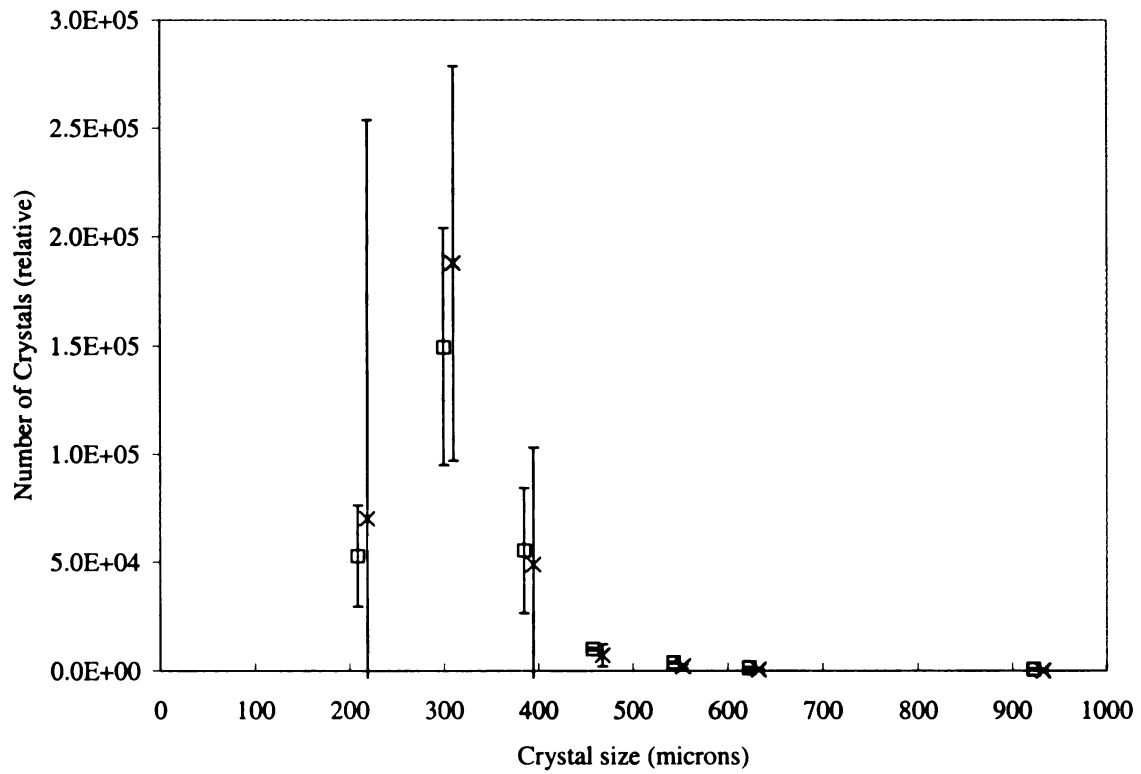


Figure 3.5

Crystal population size distribution for L-lysine monohydrochloride showing slightly larger mean size for the controlled (square) experiments versus the reference (x) crystallizations.



Figure 3.6

Photo of the L-lysine monohydrochloride crystals sampled from the 390 micron average crystal size tray (mesh #45) of the controlled crystallization.



Figure 3.7

Photo of L-lysine monohydrochloride sampled from the reference experiment (390 micron average crystal tray). Agglomerates dominate the sample with a small quantity of uniform crystals produced.

3.3 CONCLUSIONS

The probe configuration discussed provides a practical way to monitor a crystallization process *in situ* and in real time. Considering the cited potential crystal systems highlights the applicability of this approach. Monitoring the crystallization provides a means for knowing how to control it. Control is demonstrated for Lmhc where a modest increase in the mean size and a drastic improvement in the crystal quality occur.

3.4 REFERENCES

¹ LeCaptain, D. J., and Berglund, K. A., *J. of Cryst. Growth*, 203, **1999**, 561

² Delfino, M., *Mol. Cryst. Liq. Cryst.*, **1979**, 52, 271-284

³ Edited by D.S. Chemla, J. Zyss, *Nonlinear Optical Properties of Organic Molecules and Crystals Volume II*, Orlando : Academic Press, **1987**

⁴ Randolph, A. D., and Larson, M.A., Theory of particulate processes 2nd edition, Academic Press Inc., San Diego, **1988**

⁵ Mullin, J. W., Crystallization, Butterworth-Heinemann, **1993**

Chapter 4

DETECTION OF POLYMORPH CRYSTALLIZATION AND TRANSFORMATION USING SHG

Polymorphic crystalline materials pose a challenge to industrial processing, particularly in the pharmaceutical, food, and fine chemical industries, characterizing. A particular polymorph can be formed during crystallization and subsequently transform to a different polymorph, usually through solvent mediation. The nonlinear optical process of second harmonic generation (SHG) can be used to monitor polymorph formation and transformation *in situ* because each polymorph has a different second harmonic efficiency and if one polymorph has inversion symmetry no signal will be obtained at all. Ostwald's law of stages states that the least stable form appears first, thus making the transformation a concern.¹

SHG can detect crystal formation and has been demonstrated in chapters 2 and 3. Polymorph discrimination of crystal detection is used for L-aspartic and L-glutamic acid crystallization. The experiments show formation of an agglomerated crystal polymorph that is not SHG active whereas the other crystalline form is SHG active. Data are presented for polymorphic formation and transformation of crystalline L-glutamic acid.

4.1 BACKGROUND

Polymorphism started to receive extensive consideration in the 1950's with the advent of modern drug chemistry. Caution needs to be exercised when discussing polymorphs because of the tendency to mistake precipitation with polymorphism. Discussions of both are provided to avoid this misconception.

Polymorphs are identical in liquid, solution, and gas states, but differ in the crystalline solid state. These different crystal structures often have different physical properties such as melting point, density, shape, etc.² Polymorphs are of great concern in the drug industry where tableting, solubility, bioavailability, stability in suspension and overall stability are affected.³

A problematic area of polymorphism is phase transitions. The metastable form may be desired, but often transforms to a stable phase. Conversely, the stable phase may be desired in which case the transformation is needed.^{4,5,6} The transformation can occur in either the solid phase⁷ or in the solution phase. The latter is solvent-mediated phase transformation where the metastable form is able to dissolve and nucleate as the stable form.⁸

Precipitation is another method for obtaining solid material from a solution system. Unlike crystallization where a large mean crystal size is desired, precipitation results in a fine powder, which may not be crystalline. The process tends to involve relatively insoluble material, which can result in highly supersaturated solutions. This high supersaturation will favor nucleation and produce a large number of particles. Precipitation is important for finished products that need the characteristics of fine particle size. Examples include dyes and paints.⁹

Differentiation of these two separate processes is possible through a variety of methods. If the crystals are large enough to see with magnification they will have distinct straight edges and clear crystalline shapes. Additionally, crystals can diffract x-rays where a precipitate or amorphous material will not.⁹

Final consideration is given to the applicability of SHG for monitoring polymorph systems. Delfino gives a sampling of the number of biological systems that are SHG active.¹⁰ Likewise, a publication by Borcka and Haleblien lists thousands of compounds that have been reported in literature having polymorphs.¹¹ Biological molecules tend to be complex in terms of low symmetry properties, which in turn tend to crystallize without inversion symmetry. Lack of inversion symmetry is the requirement for being SHG active.

4.2 EXPERIMENTAL

Two chemical compounds, L-aspartic acid and L-glutamic acid, were chosen for this study. Both were used as purchased from Aldrich (98%) and Sigma (99%), respectfully. The measurement of SHG employs the SHG probe discussed previously in chapter 3. It is used here with no adaptations except designation of a standardization method as described in the following. Additionally, the conditions and procedure for the individual experiments used for this study are detailed in this section.

A method for standardizing the probe apparatus was developed. PMT voltage was set to 900V with 156 mW of 100 Hz. 1064 nm light measured in front of the probe. Using 62.5 grams of Spectrum KDP in 250 ml of water the output intensity was measured. Stirring rate and temperature (20°C) were held constant.

The procedure used for crystallizing L-aspartic acid is as follows. (Form B) A 1.4% wt. in water was heated to 70°C, and then cooled to 10°C. Upon reaching 10°C the time and the addition of methanol to the solution were started. The methanol addition rate was approximately 4 mL/min. The crystallization of L-aspartic acid (Form A) was accomplished by heating a 1.8% solution in water to 80°C and then cooling to 50°C. It was held at 50°C for 30 minutes and then methanol was added (~4 mL/min.) during the following time intervals; 5.4 – 6.4 min., 8.4 – 9.4 min., and 11.4 – 32.7 min.

The L-glutamic acid crystallization loosely follows previous work done by Kitamura.¹² His work depicted two different polymorphs, potential conditions for forming each, and a pathway for solvent mediated transformation. These two polymorphs were produced.

The following four procedures were used for crystallizing and transformation of the L-glutamic acid. Procedure A; a 2.4% wt/wt in water solution was heated to 70°C and then cooled to 20°C when the timer was started. At 5 minutes the addition of methanol was started at a rate of 4 mL/min. Procedure B involved heating a 2.8% solution in water to 80°C and then cooling to 45°C. The timing was started immediately and at 4.1 minutes methanol addition (~4 mL/min.) was started. Procedure C; a 3.3% wt/wt solution in water was heated to 80°C and then cooled to 45°C when the time was started. Procedure D is identical to procedure C except, the concentration was 2.8% and at time 3.1 minutes methanol was added (rate of 4 ml/min.).

The measurement of light scatter was incorporated into the experiment for comparison. Averaging the scatter from a Metrologic Neon Laser at 632.8 nm was done using the fiber optic detection of a Guided Wave Absorbance Instrument. The

crystallizer was equipped with a cell window in the side through which the HeNe laser was shown. The intensity of scattered light was measured above the solution surface using the aforementioned instrument.

The x-ray powder patterns were collected on a Rigaku instrument. The x-ray source was a copper rotating anode using the k_{α} wavelength. The values were collected at reflection θ and 2θ . Instrument settings were x-rays 100 microamps and 45 millivolts with all spectra collected at room temperature.

4.3 DATA AND DISCUSSION

Two amino acids previously known to be SHG active¹³ were chosen for the current study. The first, L-aspartic acid is crystallized in two separate experiments. The second, L-glutamic acid is crystallized using the four procedures listed above. These experiments deal with monitoring L-glutamic acid crystal formation, relative efficiency for the two polymorphs, and preliminary work towards incorporating light scattering in the analysis.

First, the SHG monitoring of L-aspartic acid crystallization was performed. Figure 4.2 shows the SHG monitoring of L-aspartic acid crystal formation, crystallized using the procedure listed in the experimental section. The crystallization follows the typical crystal formation curve when using the SHG technique as described in chapter 3. Upon completion of the experiment the solution was filtered and the crystals dried. A photograph of the resulting crystals (Figure 4.3) and x-ray data (Figure 4.8) verify that the solid is indeed crystalline.

Next, L-aspartic acid is crystallized under a second set of conditions (Form B), which results in a different polymorph. Figure 4.4 shows the second harmonic output

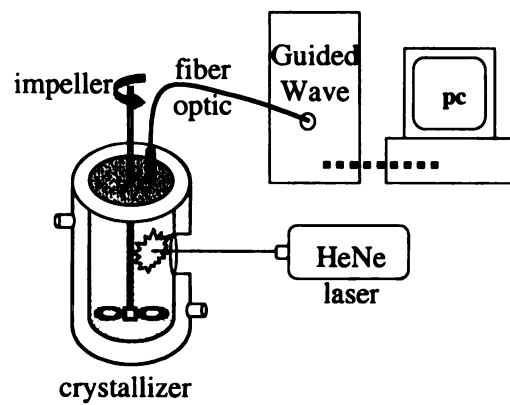


Figure 4.1

Schematic shows the light scattering set-up and equipment.

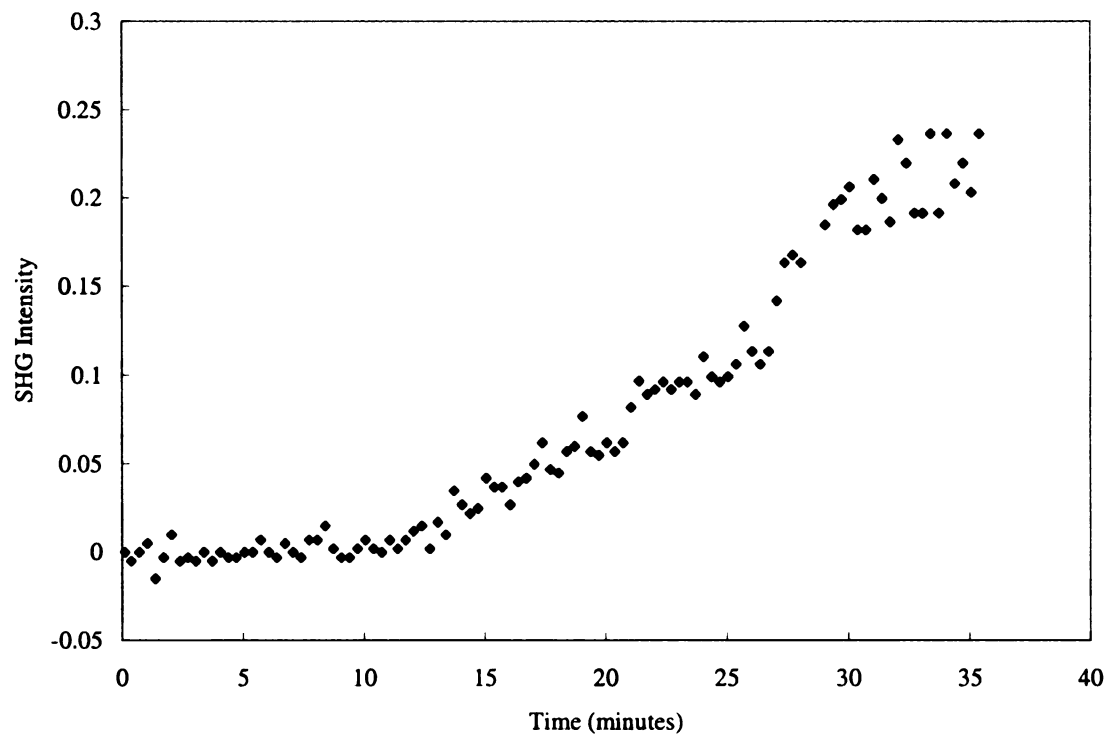


Figure 4.2

SHG signal showing the Anti-solvent (methanol) crystallization of a 1.8% wt. in water at 50°C of L-aspartic acid (Form A).

from this crystallization experiment. No discernible second harmonic signal is detected. Reference to the light scatter of a HeNe laser provides qualification of the increasing presence of solid in the solution. Light scattering (figure 4.5) shows the initial solution clouding occurs with the start of methanol addition. It then records the increase in solid formation, which starts at 25 minutes. Photograph (figure 4.6) and x-ray diffraction shown in figure 4.7 verify the difference in crystal structure. This particular crystal form does not frequency double. Either the change in crystal structure or extreme small size of the crystals results in the rapidly crystallizing form (Form B) not to be SHG active. Comparison of figure 4.3 and 4.5 proves SHG can be used for selectively detecting a particular polymorph. The crystallization of the second form (Form B) is not SHG active, therefore the difference between the two crystallizations can be detected.

The second portion of this chapter addresses polymorphic determination of L-glutamic acid polymorphs. The first experiment demonstrates using the SHG technique on L-glutamic acid crystallization. The next two experiments monitor transformations from one crystalline form to the other. The final crystallization is dedicated to groundwork in the combination of SHG monitoring with light scattering.

L-glutamic acid has two polymorphs.¹² The α form pictured in figures 4.9 and 4.10 was crystallized using procedure A from the experimental section. Figure 4.8 shows the crystal formation curve. At 17 minutes the crystal formation starts and then finishes around 25 minutes. Figure 4.9 was collected at the onset of crystallization (17.4 minutes). The photo is a mix of α crystals and other smaller particulate. Figure 4.10, collected at the completion of the crystallization shows the crystals have grown in size and the finer crystals are no longer present. The crystallization progresses from a mix of



500 μm

Figure 4.3

Photo of a sample of L-aspartic acid crystals collected after completion of the crystallization (Form A).

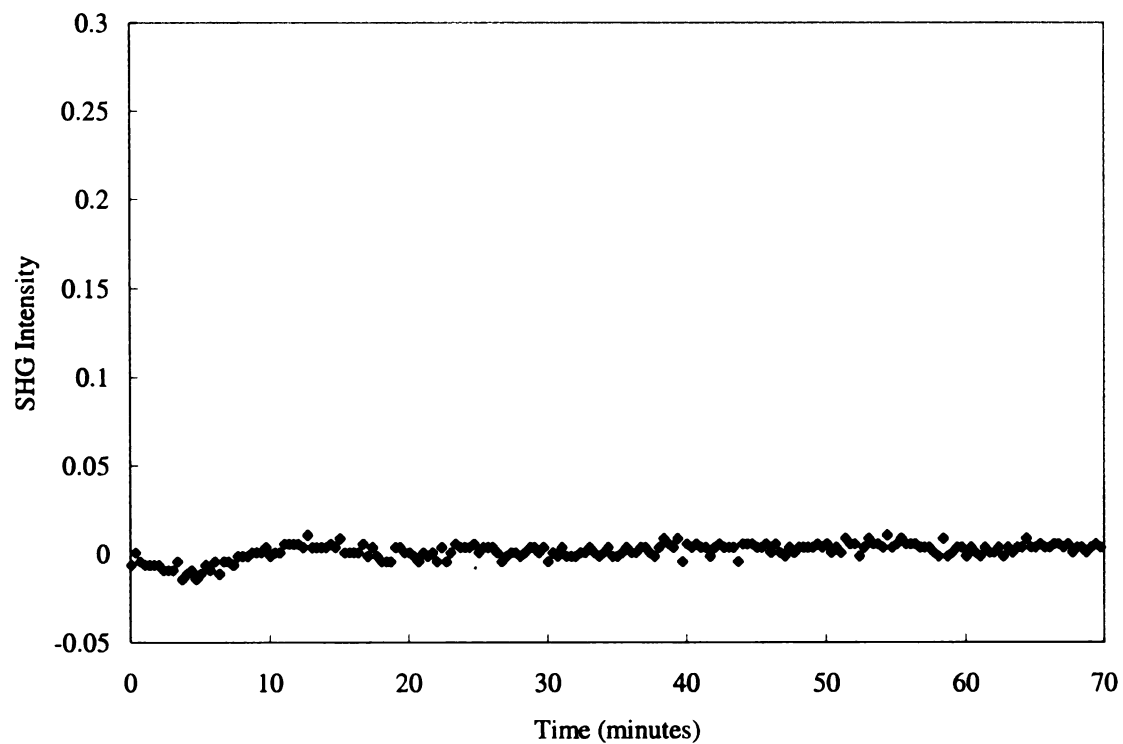


Figure 4.4

SHG output measured for the 1.4% wt. in water L-aspartic acid (Form B) anti-solvent crystallization at 10 °C. Changing optical properties of the solution causes the small fluctuation at the start. Through the course of the rapid crystallization no SHG is produced.

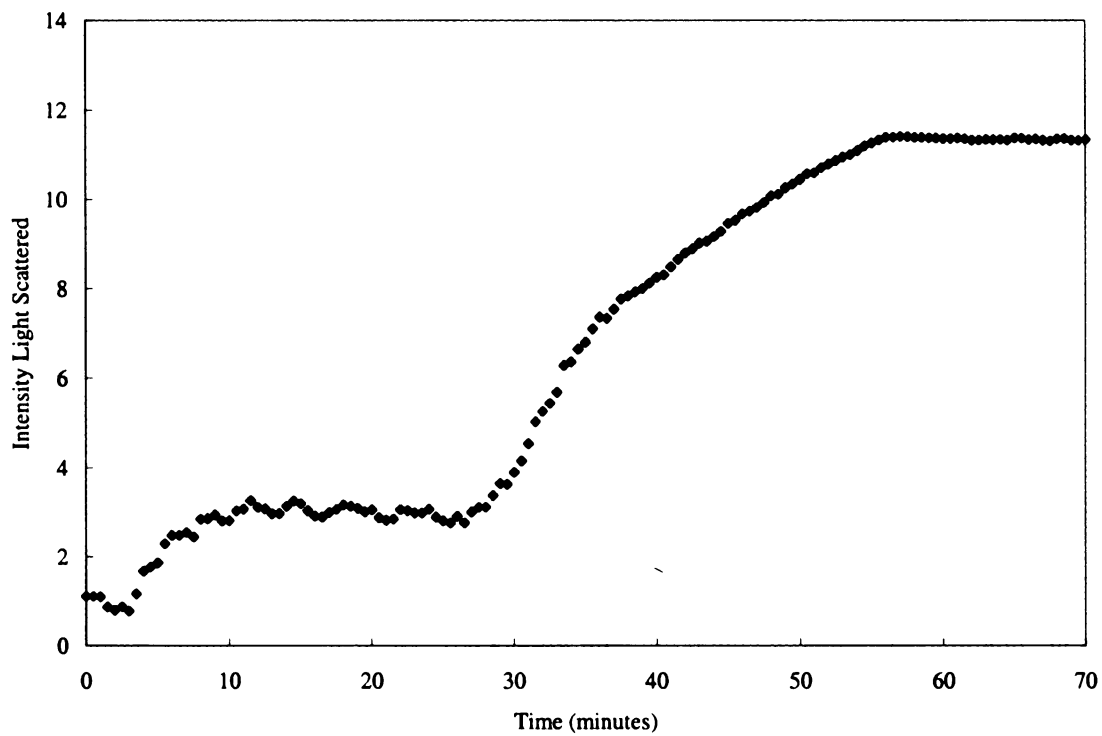


Figure 4.5

Light scattering curve for L-aspartic acid crystallization (Form B) measured simultaneously with figure 4.5. At 3 minutes methanol addition was started and at 28 minutes the crystal formation starts.

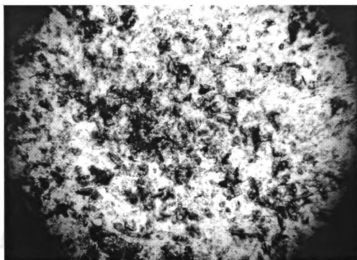


Figure 4.6

500 μm

Photo shows the L-aspartic acid crystals (Form B) taken at the completion of the second experiment. The crystals appear as a very fine powder.

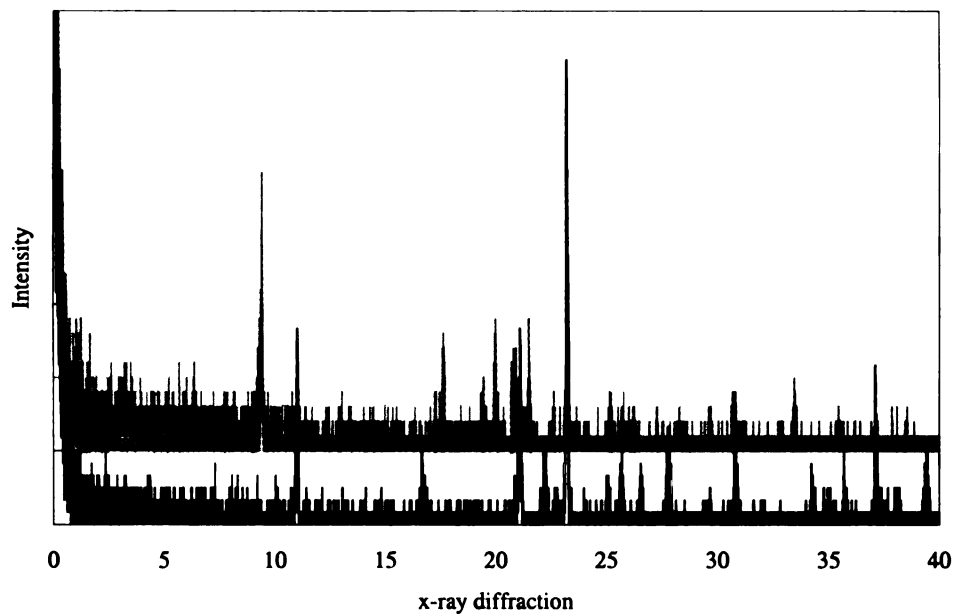


Figure 4.7

X-ray powder pattern shows the difference in the two L-aspartic acid crystals. The gray pattern (upper) corresponds to the non-SHG active crystal form (Form B, figure 4.6) and the black trace (lower) corresponds to the SHG active crystal (Form A, figure 4.2).

small particles and crystals to just crystals upon completion. The particle formation is scrutinized more closely in the following crystallization.

The importance of monitoring the transformation from one crystal form to another needs to be stressed. Most solution based techniques that measure supersaturation cannot detect transformations, nor will light scattering or visual techniques differentiate these crystals.

Two samples were collected from different times during the crystallization (procedure B), filtered, and then photographed. The final solution was also filtered and the solid photographed. Photos of the samples are shown in figures 4.12, 4.13, and 4.14 respectively. The SHG monitoring of the system is shown in figure 4.11. Note, the crystal formation occurs at approximately 35 minutes.

The first sample (50 mL) was collected at 21 minutes, figure 4.12 shows the solid that resulted after filtering and drying. A small particulate crystalline material is the only solid present, which is not SHG active (figure 4.11). The x-ray powder pattern (Figure 4.23) indicates this is the α form. At 32 minutes into the experiment crystal formation is evidenced by the SHG increase. Figure 4.13 taken at 41 minutes verifies the presence of crystals. Upon completion, the solution was filtered, dried, and photographed (figure 4.14). Like figure 4.13, this photo shows the presence of crystals. The dominant crystal form is β . The small particulate α form is not SHG active but the larger β form is.

The formation of the β polymorph of L-glutamic acid is demonstrated in Figure 4.15. Procedure C was used for this experiment. The crystal formation starts around 60 minutes. The photo shown in Figure 4.16 taken from the sample collected at 69.1 minutes shows predominantly polymorph α with slightly different shape characteristics

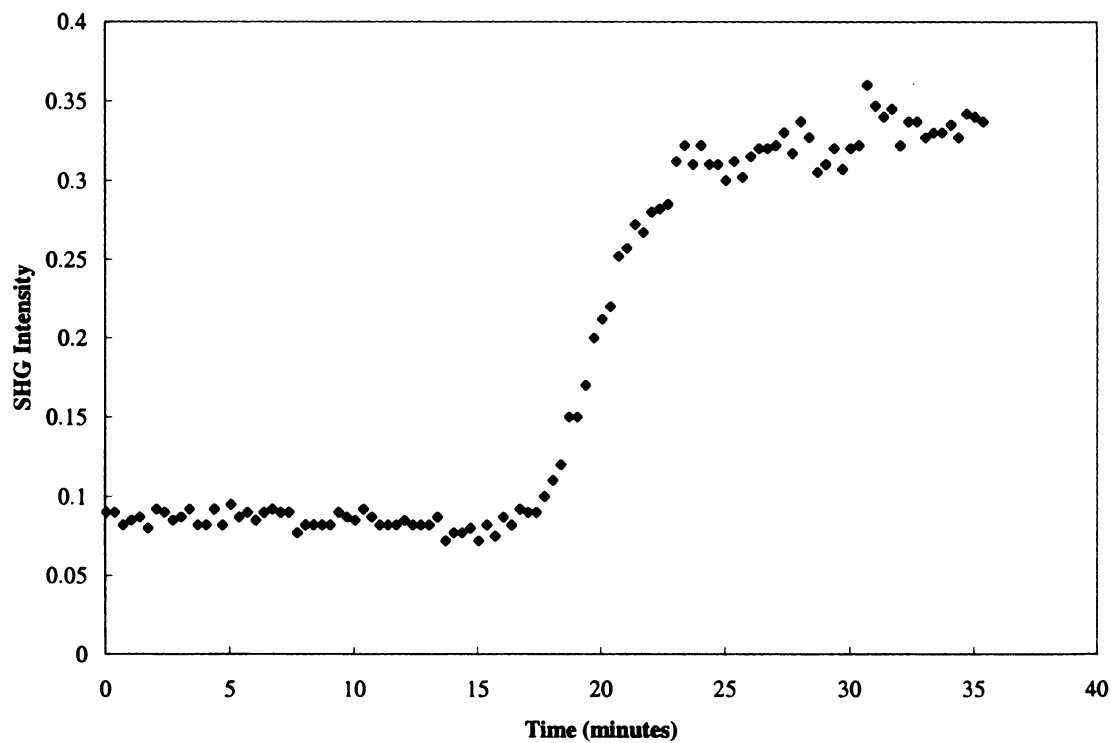
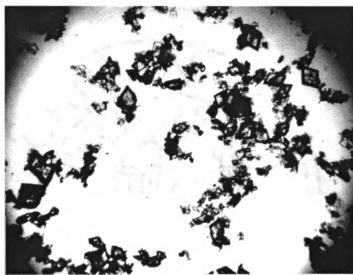


Figure 4.8

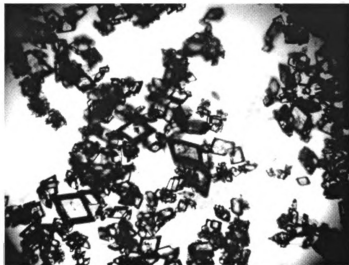
SHG crystal formation curve for the anti-solvent crystallization of 2.4% wt. in water L-glutamic acid at 20°C. Procedure A from the experimental section was used. Samples were collected and photographed at 17.4 minutes and at the completion of the experiment.



500 μm

Figure 4.9

Photo of α crystals and small particles sampled at 17.4 minutes just after the start of the L-glutamic acid crystallization.



| 500 μm |

Figure 4.10

Photo of L-glutamic acid crystals, taken at the completion of the crystallization in figure 4.8. Shows the α form of crystals.

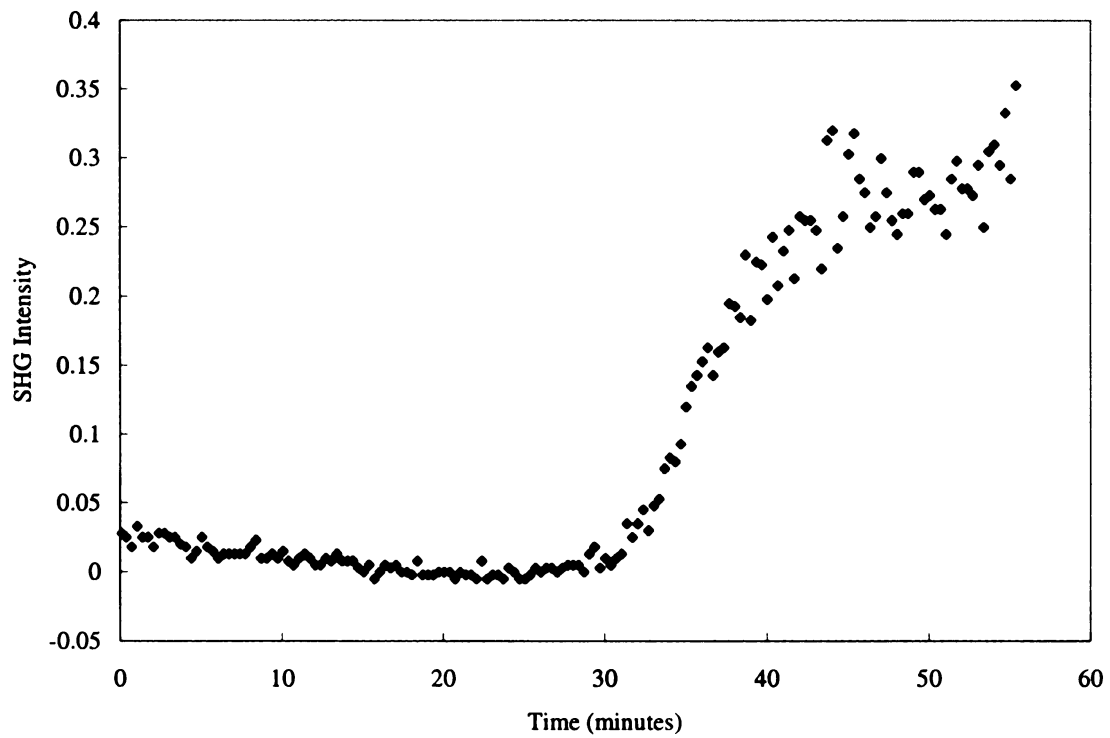


Figure 4.11

Plot shows the SHG anti-solvent crystallization of 2.8% wt. in water α -L-glutamic acid. Crystal formation starts at 32 minutes. Solution samples were taken at 21 and 41 minutes.



500 μm

Figure 4.12

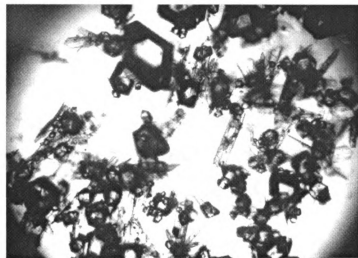
Photo of L-glutamic acid small crystals taken at 21 minutes. The crystallization curve is shown in figure 4.7. The crystals are α form as determined by x-ray (figure 4.22).



500 μm

Figure 4.13

Photo from the L-glutamic acid crystallization (Figure 4.11) sampled at 41 minutes. Shows predominantly β crystals.



500 μm

Figure 4.14

Photo from the L-glutamic acid crystallization, sample was collected upon completion of the experiment (Figure 4.11). Again, β crystals dominate.

than the previous photo. The solution was then monitored for extended time to allow solvent mediated transformation to the β form of crystals (figure 4.17). The photo is predominantly the β form. The SHG decreases over time as the crystals transform from the α to the β form. From Kitamura's work, the α form has a higher solubility than β . What can be concluded is the α form has a higher SHG efficiency. The lower the solubility of β means more β crystals are formed than with the α form yet the SHG decreased. Confirmation of the crystal morphology was done by x-ray powder diffraction (figure 4.22) and parallels Kitamura's results.¹²

The experiment indicates the polymorphs have a different SHG efficiency. The two polymorphs have identical crystal symmetry and differ on in the spacing within the crystal lattice.^{14,15}

The final crystallization procedure (D) brings to light the difficulties trying to quantify the SHG technique for two polymorphs. The crystals formed are not the clean prism shape of the low temperature anti-solvent crystallization. Rather, they are a rough hexagonal shape, pictured in figures 4.19 and 4.20. The SHG monitoring of the crystallization and simultaneous light scattering monitoring is shown in figure 4.18. Approximately 50 mL of sample were collected at 28.5 minutes and 50.5 minutes for photos 4.19 and 4.20 respectively. Figure 4.21 shows the resulting solid sampled at completion of the experiment.

These results highlight the difficulty in simultaneous monitoring with light scatter and SHG. As each sample is drawn for verification of the solution, the light scatter drops in intensity due change in solution conditions. SHG on the other hand is not affected as

much by the changes. This highlights the benefit of SHG being less prone to solution interference.

4.4 CONCLUSIONS

SHG can be used to differentiate between crystal polymorphs. *In situ* detection is possible for L-aspartic acid and L-glutamic acid crystallization. The former is crystallized separately as the two different forms. One form is SHG active while the other is not. The L-glutamic acid α crystal formation and transformation to β form, relative efficiency of the two polymorphs, and preliminary work toward the incorporation of light scattering into the SHG analysis is performed.

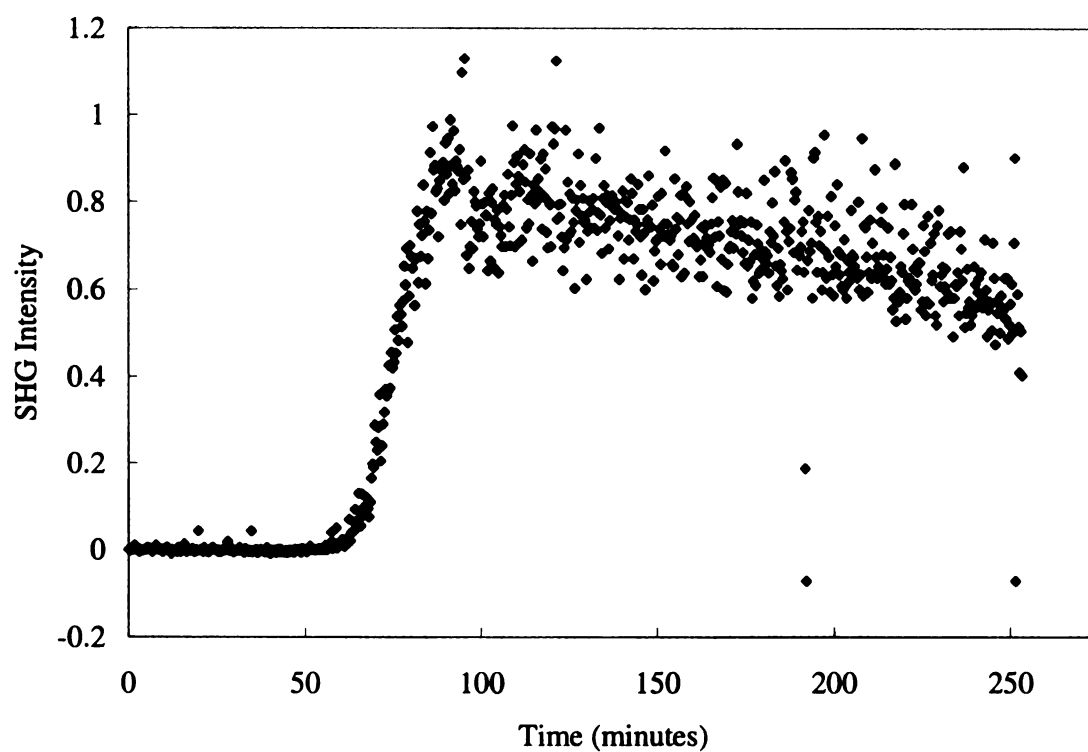
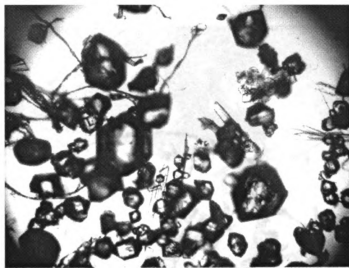


Figure 4.15

SHG crystal formation of 3.3% wt. in water L-glutamic acid at 45°C generated using procedure C. The monitoring was extended to allow for transformation from the α form to the β form.



500 μm

Figure 4.16

Photo of predominantly α -L-glutamic acid crystals collected at time 69.1 minutes from the crystallization in figure 4.15.

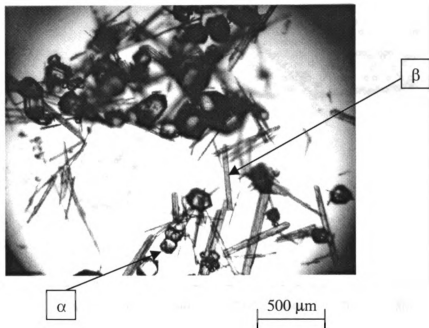


Figure 4.17

L-glutamic acid crystals collected at the end of the experiment pictured in figure 4.15. The photo shows a near equal mix of α and β crystal forms.

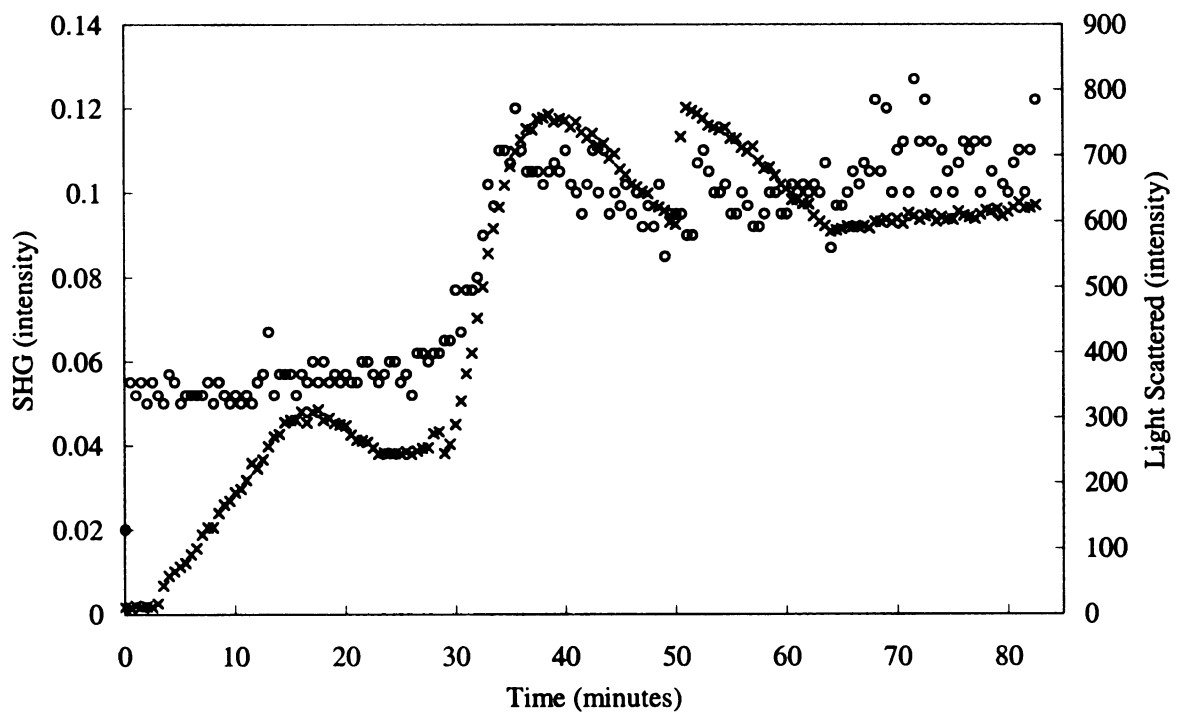
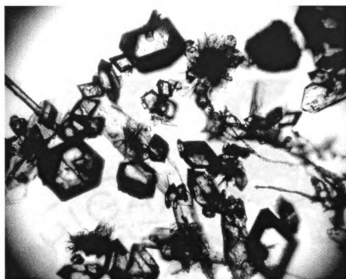


Figure 4.18

SHG (o) crystal formation and light scattering (x) plotted for L-glutamic acid formation. The crystallization parameters are described as procedure C in the experimental section. Methanol addition was started at 3.1 minutes and samples were collected at 28.5 and 50.5 minutes.



500 μm

Figure 4.19

L-glutamic acid crystals sampled at 28.5 minutes. The crystals are a mix of small particulate and α polymorph (prism) with a small amount of the β form (needles).

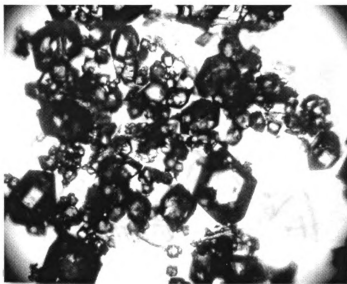
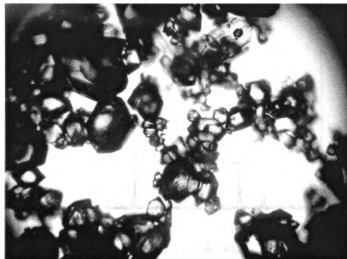


Figure 4.20

500 μm

L-glutamic acid crystal photographed at 28.5 minutes. The crystal shape is predominantly the α polymorph.



500 μm

Figure 4.21

L-glutamic acid crystals collected at the completion of the experiment.
Crystal shape is the prismatic α polymorph.

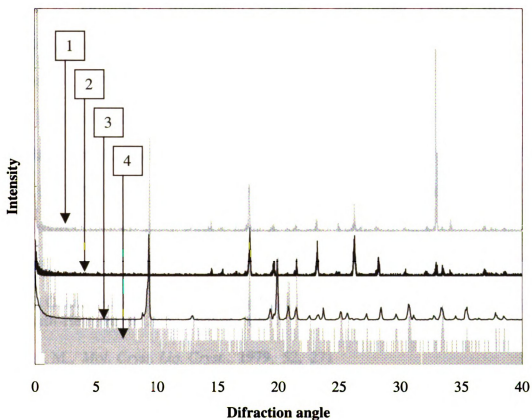


Figure 4.22

X-ray powder patterns for L-glutamic acid. Pattern 1 is crystals collected from crystallizations of α form crystallization 4.11, pictured in figure 4.13. Pattern 2 is prism shape (α form) and pattern 3 is the needle shape as referenced.¹² Pattern 4 is crystals collected from 4.11 crystallization and pictured in figure 4.12.

4.5 REFERENCES

- ¹ Ostwald, W., Grundriss der Allgemeinen Chemie, W. Engelmann, Leipzig, **1899**
- ² Haleblian, J. and McCrone, W. *J. Pharm. Science*, **1969**, 58, 911
- ³ Haleblian, J., *J. Pharm. Science*, **1975**, 64, 1269
- ⁴ Davey, R. J. and Richards, J., *J. of Cryst. Growth*, **1985**, 71, 597
- ⁵ Matsuda, K. et. al., *J of Pharm. And Pharmacology*, **1992**, 44, 678
- ⁶ Davey, R. J., Guy, P. D., and Ruddick, A. J., *J. of coll. and Inter. Sci.*, **1984**, 73, 173
- ⁷ Kitaigorodsky, A. I. et. al., *J. Phys. Chem. of Solids*, **1965**, 26, 463
- ⁸ Cardrew, P. T. and Davey, R. J., *Proc. Royal Soc. London A*, **1985**, 398, 911
- ⁹ Sohnel, O. and Garside, J., Precipitation Basic Principles and Industrial Applications, Butterworth-Heinemann LTD., Oxford, **1992**
- ¹⁰ Delfino, M., *Mol. Cryst. Liq. Cryst.*, **1979**, 52, 271
- ¹¹ Borka, L. and Haleblian, J., *Acta. Pharm. Jugosl.*, **1990**, 40, 71
- ¹² Kitamura, M., *J. Crystal Growth*, **1989**, 96, 541
- ¹³ Riechoff, K. E. and Peticolas, W. L., *Science*, **1964**, 147, 610
- ¹⁴ Hirayama, N. et. al., *Bull. Chem. Soc. Jpn.*, **1980**, 53, 30
- ¹⁵ Lehmann, M. S., Koetzle, T. F., and Hamilton, W. C., *J. Cryst, Mol. Struct*, **1972**, 2, 225

Chapter 5

ENANTIOMERIC CRYSTAL DETERMINATION USING SHG

Mixed crystallization systems, where more than one enantiomer is present are important in the production of chiral compounds. The similarity between enantiomers is very important particularly in pharmaceuticals. The motivation is *in situ* determination in production of chiral chemicals for pharmaceuticals. This chapter focuses on using SHG to differentiate between a single enantiomer and conglomerate crystallization.

5.1 BACKGROUND

The term “enantiomer” describes the relationship between two different molecules. The molecules are identical in atoms present and the bonding of these atoms. The difference is in the physical arrangement or physical structure. Enantiomers are mirror images of each other, which are not superimposable.¹ The existence of enantiomeric molecules has been recognized since the early days of organic chemistry. Enantiomers crystallized such that both are in the same crystal lattice are a conglomerate. Pasteur recognized the first example of a conglomerate formation in ammonium tartrate crystals.²

Naturally occurring molecules tend to be exclusively one enantiomer whereas synthetic production tends to produce racemic mixtures. Separation of these mixtures is possible using crystallization. By seeding a supersaturated solution with a specific

enantiomer, that enantiomer may crystallize preferentially.³ A number of compounds have been studied to determine mechanisms for conglomerate formation.^{4,5,6} Characteristics of general crystal structures has been attempted with general trends seen in the hydrogen bonding.⁷ Though no clear mechanistic theory applies. A variety of physical methods have been used for determination of crystal form. Fractional crystallization using a chiral resolving agent is the most common, along with FTIR, Raman, and physical data such as optical rotation and melting point.^{3,8}

5.2 EXPERIMENTAL

The L-aspartic acid (98% purity, Aldrich) and DL-aspartic acid (98% purity, Aldrich) were used as received from the supplier. The SHG apparatus used is described in chapter 3 with the modifications described in chapter 4.

Crystallization of the L-aspartic acid was carried out as follows. A 1.9% wt/wt solution in water was heated to 80°C, cooled to 30°C when the time was started. Methanol was added as the anti-solvent at a rate of ~2 mL/min. between 9.7 and 11.7 minutes. The flow rate was increased to ~4 mL/min and was added from 29.1 minute to 31.1 minutes.

The DL-aspartic acid crystallization was done by taking a 3.1% wt/wt in water solution, heating it to 80°C, and then cooling to 50°C when the timer was started. Methanol was again added as the anti-solvent from 5.1 – 13 minutes (rate of ~2 mL/min.) and 13 – 37 minutes (rate of ~ 4 mL/min.).

5.3 DATA AND DISCUSSION

The two investigations carried out here focus on enantiomeric and polymorphic detection. L-aspartic and DL-aspartic acid are crystallized. The experimental section underscores the complexity of the crystallization procedures. As the complexity of the crystallization increases efficient SHG monitoring becomes now useful.

SHG can distinguish enantiomerically pure L-aspartic acid crystals from DL-aspartic acid crystals. The SHG crystallization monitoring for L-aspartic acid is shown in Figure 5.1. Crystals start forming at 15 minutes and continue until 20 minutes, when the SHG no longer increases. The photo in figure 5.2 shows a sample of the crystals after filtering and drying.

Next, the racemic mixture of DL aspartic acid was crystallized. Figure 5.3 shows the SHG monitoring. The DL aspartic acid is not SHG active, therefore no second harmonic is generated. For proof, after completion of the experiment, the crystals were filtered and dried. The crystal size is again fairly small (Figure 5.4), but notably larger from the L form crystallized above. The photo shows very distinct crystal shapes. Comparison of the previous two crystallizations demonstrates how SHG can distinguish between a crystalline racemic mixture and chirally pure form of aspartic acid. For example synthetic pathways to manufacturing enantiomeric material often times does not selectively produce a pure enantiomer. SHG could be used *in situ* to determine the particular crystal forming. The enantiomerically pure crystal and the conglomerate have identical crystal symmetries except for the number of molecules in the lattice. DL aspartic acid has 8 whereas L aspartic acid only has 4.^{9,10} This is supported by the data of the L form being SHG active and DL form is not.

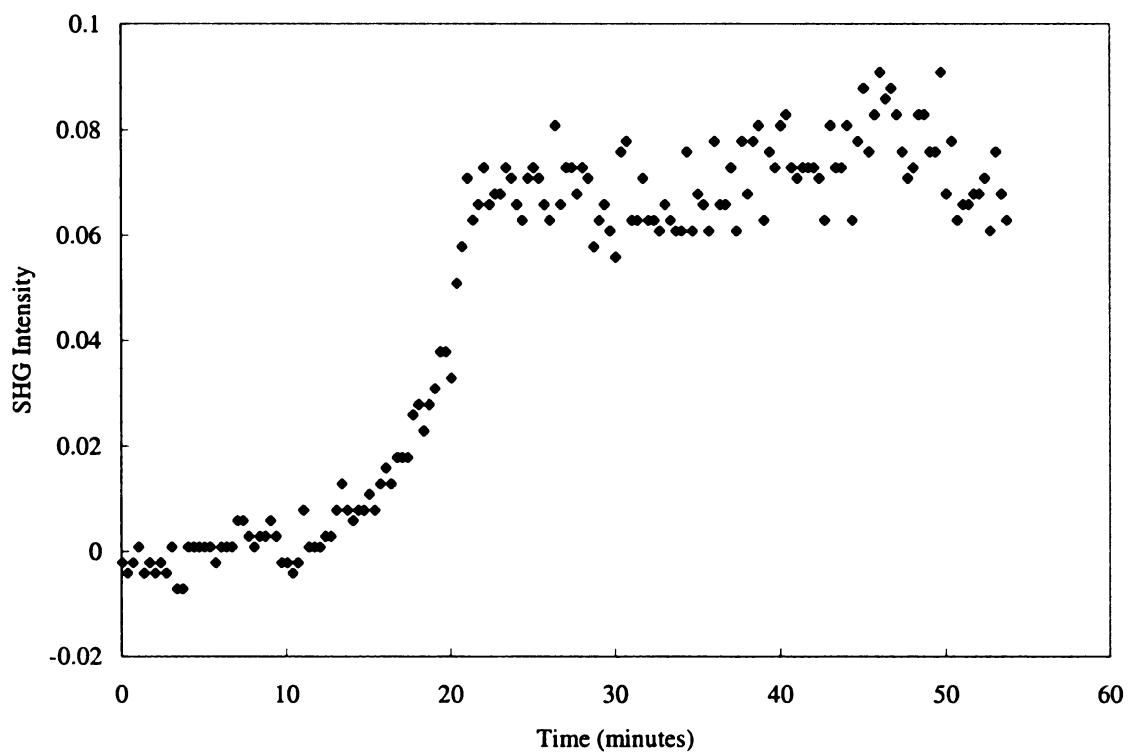
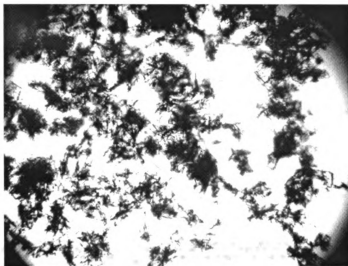


Figure 5.1

The SHG crystal formation curve for L-aspartic acid. Crystal formation starts at ~15 minutes and reaches depletion of the supersaturation at 23 minutes. Methanol as the anti solvent was used on this 1.9% wt/wt solution crystallized at 30 °C.



500 μm

Figure 5.2

Photograph of L-aspartic acid crystals collected after the completion of the crystallization performed in figure 5.1. The crystals are rather small and difficult to fully contrast in this photo reproduction.

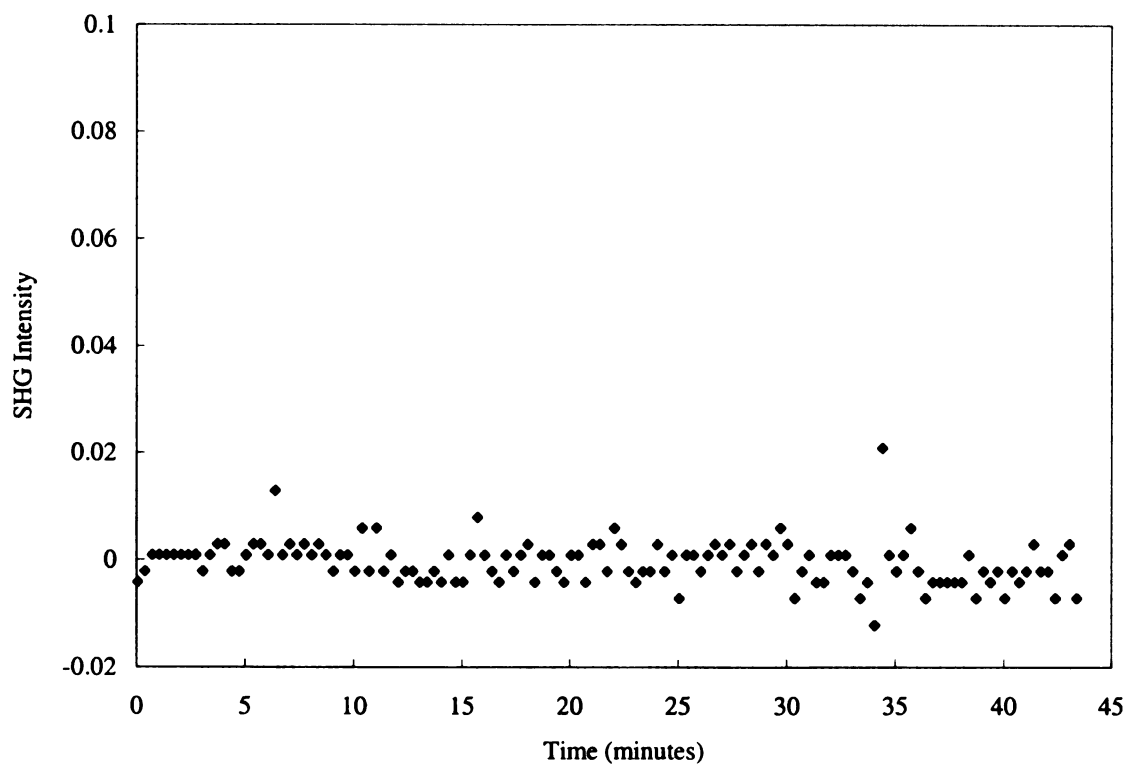


Figure 5.3

SHG monitoring of 3.1% wt/wt DL-aspartic acid methanol anti solvent crystallization at 50 °C. No second harmonic is detected, but crystals are present as evidenced by the photo in figure 5.4.

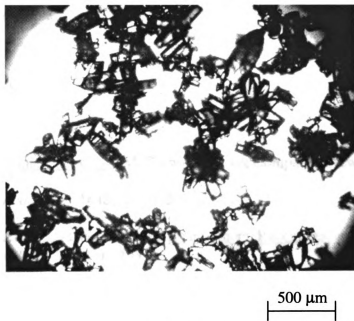


Figure 5.4

DL-aspartic acid crystals photographed upon completion of the crystallization. Distinct crystal shapes are present.

5.4 CONCLUSIONS

In situ determination of enantiomer or polymorph is crucial for efficient batch crystallization. Ease of sampling and response time of SHG makes it applicable to such experiments. L-aspartic acid can be differentiated from DL aspartic acid crystallization using the SHG technique.

5.5 REFERENCES

- ¹ Carey, F. A., Organic Chemistry, McGraw-Hill Book Company, New York, 1987
- ² Pasteur, L. C., *Acad. Sci.*, 1848, 26, 535
- ³ Jacques, J., Collet, A., and Wilen, S. H., Enantiomers, Racemates, and Resolutions, Krieger Publishing Co., Malabar, 1994
- ⁴ Kosma, D., Boeskei, Z., Simon, K., and Foggasy, E., *J. Chem. Soc., Perkin Trans.*, 1994, 2, 1883
- ⁵ Larson, S. and Marthi, K., *Acta. Crystallogr.*, 1995, B51, 338
- ⁶ Ung, A. T. et. al., *J. Am. Chem. Soc.*, 1995, 117, 8745
- ⁷ Kazushi, K., et. al., *J. Am. Chem. Soc.*, 1996, 118, 3441
- ⁸ Kozma, D., Maria, A., and Eemer, F., *Tetrahedron*, 1994, 50, 6907
- ⁹ Rao, S. T., *Acta Cryst.*, 1973, B29, 1718
- ¹⁰ Derissen, J. L., endeman, H. J., and Peerdeman, A. F., *Acta. Cryst.*, 1968, B24, 1349

Chapter 6

FUTURE WORK; SECOND ORDER NONLINEAR OPTICAL CHEMICAL SENSORS

6.1 INTRODUCTION

There are many different types of chemical sensors, ranging from pH meters to thermistors. Sensors are small, sometimes robust devices capable of responding to a change in analyte concentration or system condition. Most common spectrochemical sensors rely on absorbance, reflectance, or luminescence.¹ Sensitivity and selectivity are of key importance. The continued work could use second harmonic generation (SHG) in the construction of a more sensitive and selective chemical sensor.

6.2 BACKGROUND

Sensors are composed of two separate components, the transducer and the sensing region. The transducer translates the change in "signal" to a meaningful value. Commercial modules exist for this portion making it inexpensive, small, and very robust. The second area is the sensing region, which needs to be small, robust, and chemically selective. The size and robustness for this specific sensor type are obtainable because of current fiber optic and light detection technology.¹

The applicability of SHG for chemical sensing relates directly to the number of interfaces and surfaces available for study. An extensive review by Corn and Higgins examines SHG measurements from liquid – liquid, gas – solid, and liquid – solid interfaces.² The chemical sensor would implement an interface for the sensing area. For example, immobilizing an antibody onto a substrate would make that surface selective to a particular antigen. The change at the surface due to this binding could then be measured using SHG. The surface sensitivity and specificity of the measurement would be the advantages of the sensor. The large number of interface applications being studied creates a large variety of potential sensor applications.

The SHG sensor has certain equipment considerations. SHG is a nonlinear optical technique, therefore it requires a monochromatic, high intensity light source. Nanosecond or shorter laser pulse widths are adequate. Laser technology and availability has substantially increased in recent years making small relatively inexpensive diode pumped lasers available. The remaining portion of the sensor (see diagram), optics, detector, and electronics for the transducer are available commercially.

6.3 EXPERIMENTAL

This section presents two pathways for investigating the SHG chemical sensor. The first relies on a liquid-solid interface for the sensing region to differentiate enantiomers. The second would use SHG circular dichroism to measure enantiomeric or potentially polymorphic differences at a liquid – air interface.

Enantiomeric detection

This slight difference in orientation of enantiomers is known to inhibit crystal formation and crystal growth differently for similar chemical compounds. Gases and March have

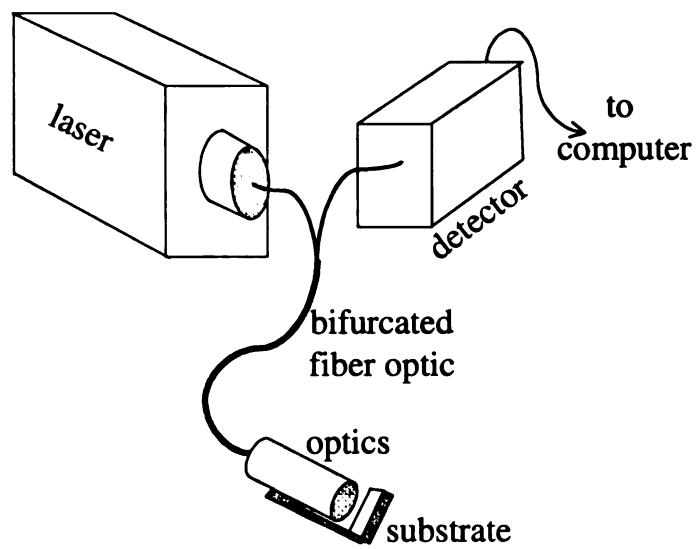


Figure 6.1

The schematic of an SHG sensor.

demonstrated this phenomenon on the inhibition of L-glutamic acid crystal formation by L-lysine. D-lysine does not inhibit the L-glutamic acid crystallization. These studies were done in bulk solutions, measuring the crystal formation by using a light scattering technique.³ However, crystal formation is a very complicated process that is difficult to control. Crystal growth on the other hand is better understood. By immobilizing the L-glutamic acid on the substrate, the presence of L-lysine would alter the crystal growth, changing the crystal structure, producing a change in SHG. The quantity of L-lysine would be measured without interference from the D form. Clearly, the opportunity to investigate other enantiomeric combinations exists.

Polymorphic determination

A second project is detection of enantiomeric and polymorphic differences. Polymorphs are identical chemically, differing only in the crystal structure. By using circular difference SHG, selectivity of the enantiomers and polymorphs is achievable. SHG circular difference is analogous to linear circular dichroism, but is more sensitive. Verbiest and coworkers have demonstrated this SHG circular dichroism on bacteriorhodopsin at an air - water interface.⁴ Here again, a vast number of polymorphs and enantiomers exist for potential sensing applications.

6.4 CONCLUSION

Potential applications in the fields of industrial process control and environmental sensing exist. Validation of this proposed technique would be necessary. Raman spectroscopy and X-ray diffraction would be the primary methods of verifying and calibration of this technique.

6.5 REFERENCES

- ¹ Cattrall, R. W., *Chemical Sensors*, Oxford Science Publications, Oxford, **1997**, Chaps. 1-3
- ² Corn, R. M., and Higgins, D. A., *Chem. Rev.*, **1994**, 94, 107
- ³ Grases, F. and March, J. G., *Trends in Analytical Chemistry*, **1996**, 10, 190
- ⁴ Verbiest, V., Kauranen, M., Persoons, A., Ikonen, M., Kurkela, J., and Lemmetyinen, H., *J. Am. Chem. Soc.*, **1994**, 116, 9203

CONCLUSION

DEVELOPMENT OF SECOND HARMONIC GENERATION AS A TOOL FOR MONITORING CRYSTALLIZATION

Monitoring crystallization provides a means for knowing how to control it. The goal of this research project was to develop an *in situ* probe for monitoring crystallization. The ability to monitor crystal formation enables better control of the crystallization process. The development of SHG as a way of monitoring the crystallization process is an excellent complementary tool to the methods already developed.

The work is laid out roughly in the order of development. The exception is Chapter 1, which dealt with monitoring crystallization, but employs the use of Raman spectroscopy instead of SHG. By considering the practicality, benefits, and limits of this technique on the laboratory scale, potential application to industrial scale can be realized. Raman spectroscopy is an optical technique that can be performed *in-situ* and within the time frame of the crystallization phenomena of selected chemical systems.

The initial demonstration and proof of the applicability of the SHG technique as a method for monitoring crystal formation in supersaturated solutions is demonstrated. The advantages over turbidometric methods are shown. Refinements to the sampling technique are made and demonstrated for enhancing the crystallization of lysine

monohydrochloride. A modest increase in the mean crystal size and a drastic change in the crystal quality occurs when controlling the crystallization.

The versatility of the SHG monitoring technique is shown for polymorphic and enantiomeric detection. SHG can be used *in situ* for L aspartic acid and L-glutamic acid polymorph crystallizations and transformations for the latter. Additionally, SHG can distinguish the enantiomerically pure crystallization versus conglomerate formation of aspartic acid.

APPENDIX

Table A.1

induction time	886	917	886/917	normalized anion/crystal
0.41	194.00	58.00	3.34	0.98
1.02	194.00	58.00	3.34	0.98
1.63	194.00	58.00	3.34	0.98
2.25	194.00	58.00	3.34	0.98
2.86	197.00	60.00	3.34	0.98
3.47	197.00	60.00	3.28	0.96
4.09	197.00	60.00	3.28	0.96
4.70	197.00	60.00	3.28	0.96
5.31	197.00	60.00	3.28	0.96
5.93	197.00	60.00	3.28	0.96
6.54	197.00	60.00	3.28	0.96
7.15	197.00	60.00	3.28	0.96
7.77	197.00	60.00	3.28	0.96
8.38	197.00	60.00	3.28	0.96
9.00	200.00	61.00	3.28	0.96
9.61	200.00	61.00	3.28	0.96
10.22	200.00	61.00	3.28	0.96
10.84	200.00	61.00	3.28	0.96
11.45	200.00	61.00	3.28	0.96
12.06	200.00	61.00	3.28	0.96
12.68	200.00	61.00	3.28	0.96
13.29	200.00	61.00	3.28	0.96
13.90	200.00	61.00	3.28	0.96
14.52	200.00	61.00	3.28	0.96
15.13	201.00	61.00	3.28	0.96
15.74	201.00	61.00	3.30	0.96
16.36	201.00	61.00	3.30	0.96
16.97	201.00	61.00	3.30	0.96
17.58	201.00	61.00	3.30	0.96
18.20	201.00	61.00	3.30	0.96
18.81	201.00	61.00	3.30	0.96
19.42	201.00	61.00	3.30	0.96
20.04	201.00	61.00	3.30	0.96
20.65	201.00	61.00	3.30	0.96
21.27	201.00	61.00	3.30	0.96
21.88	201.00	61.00	3.30	0.96
22.49	201.00	61.00	3.30	0.96
23.11	201.00	61.00	3.30	0.96
23.72	201.00	61.00	3.30	0.96

Table A 1 (continued)

induction time	wavenumber			normalized anion/crystal
	886	917	886/917	
24.33	201.00	61.00	3.30	0.96
24.95	201.00	61.00	3.30	0.96
25.56	201.00	61.00	3.30	0.96
26.17	201.00	61.00	3.30	0.96
26.79	201.00	61.00	3.30	0.96
27.40	200.00	61.00	3.30	0.96
28.01	185.00	56.00	3.28	0.96
28.63	154.00	45.00	3.30	0.97
29.24	122.00	37.00	3.42	1.00
29.85	101.00	33.00	3.30	0.96
30.47	83.00	28.00	3.06	0.89
31.08	69.00	25.00	2.96	0.87
31.69	56.00	22.00	2.76	0.81
32.31	45.00	19.00	2.55	0.74
32.92	38.00	19.00	2.37	0.69
33.54	32.00	17.00	2.00	0.58
34.15	28.00	17.00	1.88	0.55
34.76	26.00	16.00	1.65	0.48
35.38	24.00	16.00	1.63	0.47
35.99	22.00	15.00	1.50	0.44
36.60	22.00	16.00	1.47	0.43
37.22	21.00	15.00	1.38	0.40
37.83	21.00	15.00	1.40	0.41
38.44	20.00	15.00	1.40	0.41
39.06	19.00	15.00	1.33	0.39
39.67	19.00	14.00	1.27	0.37
40.28	18.00	14.00	1.36	0.40
40.90	18.00	14.00	1.29	0.38
41.51	18.00	14.00	1.29	0.38
42.12	17.00	13.00	1.29	0.38
42.74	18.00	14.00	1.31	0.38

Table A.2

% supersaturation	KDP Induction times			
13.26	1.50	4.20	4.33	3.34
12.00	6.67	6.67	13.67	9.00
10.40	6.17	11.17	9.17	8.83
9.00	10.17	18.67	16.17	15.00
7.96	9.67	42.67	32.17	28.17
6.58	31.17	40.17	16.17	29.17
5.55	47.17	40.17	86.17	57.83

Table A. 3

Crystal		number of crystals			
		cont.		uncont.	
size-5	size +5	ave.	std dev	ave.	std dev
922.5	932.5	734.45115	297.84759	223.0356	203.9142
622.5	632.5	1548.7506	293.0588	721.2872	234.1405
542.5	552.5	3832.3789	377.89957	2191.088	951.4569
457.5	467.5	10144.979	557.20486	7283.248	5110.062
384.5	394.5	55507.45	28933.435	48959.4	54214.4
299.5	309.5	149451.13	54496.152	187822.3	90831.53
208.5	218.5	52900.897	23373.993	70139.98	183585.8

MICHIGAN STATE UNIV. LIBRARIES



31293018127153